A NEW CHRONOSTRATIGRAPHIC FRAMEWORK FOR EAGLE FORD- AND AUSTIN CHALK-EQUIVALENT STRATA IN WEST TEXAS: IMPLICATIONS FOR BASIN EVOLUTION AND DIACHRONEITY IN UNCONVENTIONAL RESERVOIRS

A Thesis

by

ERIC JAMES PEAVEY

Submitted to the Office of Graduate and Professional Studies of
Texas A&M University
in partial fulfillment of the requirements for the degree of

MASTER OF SCIENCE

Chair of Committee,	Michael C. Pope
Co-Chair of Committee,	Brent V. Miller
Committee Member,	Debbie J. Thomas
Head of Department,	Michael C. Pope

August 2017

Major Subject: Geology

ABSTRACT

The Ernst Member within Big Bend National Park (BBNP), Brewster County, Texas provides unique opportunities for high-resolution chronostratigraphic study of Eagle Ford-equivalent strata across west Texas and northeastern Mexico, and is partially equivalent to the Eagle Ford Group in south and central Texas where it is a prolific, unconventional shale play.

A new chronostratigraphic framework integrating three U-Pb Chemical Abrasion-Isotope Dilution Thermal Ionization Mass Spectrometry (CA-IDTIMS) bentonite ages from the Ernst Member and six bentonite ages from the Eagle Ford Group at Lozier Canyon with biostratigraphic proxies, hand-held spectral gamma ray (HHSGR), hand-held X-Ray Fluorescence (HHXRF) and $\delta^{13}C_{carb}$ measurements constraining (spatially and temporally) stratal surfaces, isotopic events and biozones in west Texas is presented. New ages for the Ernst Member type section in Ernst Tinaja, BBNP include 97.49 ± 0.12 Ma at 0.3 m (0.9 ft), 95.99 ± 0.15 Ma at 7.5 m (24.6 ft) and 91.16 ± 0.16 Ma at 52.1 m (171 ft) above the Buda Limestone/Ernst Member contact.

In BBNP, the Ernst Member preserves neither the OAE2 positive carbon isotope excursion (CIE) nor the Cenomanian/Turonian (C/T) boundary. Chemostratigraphic analysis of U, Mo, V, Zr, Ti, Ca, Sr, K, Al and Si/Ti identify a low-TOC, carbonate-rich interval (0–4.8 m; 0–15 ft), a high-TOC interval (4.8–27.4 m; 15–90 ft), the OAE2 recovery period (27.4–33 m; 90–108 ft), Langtry Member-equivalent deposits (33–52.7 m; 108–173 ft) and, bounded by the Early Coniacian *Allocrioceras hazzardi* Zone above and bentonite age of 91.16 ± 0.16 Ma at 52.1 m (171 ft) below, a Late Turonian Austin

Chalk-equivalent section (52.7–84.6 m; 173–277.5 ft) at Ernst Tinaja. Averaged correlation (COR)-derived sedimentation rate estimates range from 0.34–2.3 cm/kyr for Lower Eagle Ford-equivalent strata, 0.75–2.24 cm/kyr for Upper Eagle Ford-equivalent strata and 1.8–3.64 cm/kyr for Austin Chalk-equivalent strata.

DEDICATION

I dedicate this thesis to my parents, whose unfettered love and support has enabled me to pursue a career in the energy industry.

ACKNOWLEDGEMENTS

I'd like to thank Mike Pope for his valuable guidance in the synthesis of this manuscript, his mentorship and for the many discussions we've shared. I'd also like to thank Debbie Thomas and Brent Miller for their edits and thoughtful discussions, which significantly improved this manuscript. I'd also like to thank Jacob Thompson, Sean Borremans and Ivan Purwamaska for their assistance in the collection of ash beds and measuring of stratigraphic sections. I'd like to thank Grant Bonnette, Fernando Pachuca and Clayton Merrill for their field assistance related to collection of HHSGR data, and Matthew Wehner, Art Donovan, Jason Lundquist, Scott Staerker and Mike Pope for their assistance in measuring sections and in field sampling. Many thanks to Brent Miller for his efforts towards the back-end processing of bentonites and data reduction of ages in the laboratory. I must thank Harold Johnson, Jacob Thompson, Brandon Geddie, Claudia Riog and Vicky Gao for lab training. I'd also like to extend my sincerest gratitude to Luz Romero for her generous, prompt assistance in the laboratory.

I must also thank Don Corrick (Geologist), Diana Edwards (no longer with NPS) and Dave and Barbara (Bunny) Larson at the National Park Service (Big Bend National Park) for their help during the collection permit approval process and for their kindness and support during my many research trips to the park.

I thank Dr. Christopher Wood, Jan Jackson, Tiffany Galvan, Aeron Green, Vinetta Porter and Elizabeth, John and Alexandra Frenzel for the expediency and quality of care I received at M.D. Anderson during the latter six months of this project.

But most of all I wish to extend my eternal thanks and love to my parents, Stephen and Teresa Peavey, who have unconditionally supported my ambitious educational endeavors over the years. Lastly, I'd like to extend my thanks to my Aggie friends and family as well as my friend Dr. Cynthia R. Coron, who facilitated and nurtured the spark of ambition in me to pursue a career in the energy industry.

CONTRIBUTORS AND FUNDING SOURCES

Contributors

This work was supported by a thesis committee consisting of Professors Michael C. Pope [Adviser, Chair] and Brent V. Miller [Co-Chair] of the Department of Geology and Geophysics and Interim Dean of the College of Geosciences, Debbie Thomas [Committee Member] of the Department of Oceanography.

Foraminifera were prepped by Eric Peavey and analyzed by Jason Lundquist (consultant). Calcareous nannofossils were prepped and analyzed by Scott Staerker (consultant). HHXRF analyses were conducted by Matthew Wehner, CA-IDTIMS lab support given by Brent V. Miller and $\delta^{13}C_{carb}$ data by Chris Maupin at the SIGF Laboratory at Texas A&M University. Field work assistants are noted in the acknowledgements.

All other analytical work conducted, including generation of figures, tables and interpretations presented for this thesis were completed by the student independently, save for editing contributions by Michael C. Pope, Brent V. Miller and Debbie Thomas.

Funding Sources

This project was funded in part by the W.L. Calvert Scholarship (via Houston Geological Society), Unocal Graduate Fellowship in Geoscience (via Texas A&M University) and Chevron Corporation; these funds have partially paid for field expenses and the entirety of costs associated with nannofossil (Atlantes Geoconsulting, Inc.) and stable isotope (SIGF Laboratory, Texas A&M University) analyses.

TABLE OF CONTENTS

Page

1. INTRODUCTION

High-resolution U-Pb zircon geochronology was used to link magmatic activity (volcanism) and extinction (Blackburn et al., 2013), constrain stratigraphic intervals (Bowring et al., 2006; Desmares et al., 2007; Eldrett et al., 2015; Mattinson, 2011, 2013; Meyers et al., 2001) and determine orbital forcing in sedimentation (Hays et al., 1976; Meyers, 2012; Meyers et al., 2012; Meyers and Sageman, 2007; Wu et al., 2013). This project utilizes U-Pb zircon geochronology of ash beds from two measured sections of the Boquillas Formation (Figure 1) and biostratigraphic proxies (e.g., foraminifera) to temporally constrain deposition of the Ernst Member of the Boquillas Formation in Big Bend National Park (BBNP). This study also uses HHSGR, HHXRF, $\delta^{13}C_{carb}$ stable isotopes and lithostratigraphy from measured sections (Gardner et al., 2013; Moore 2016; Wehner et al., 2015), biostratigraphic data from Moore (2016), Corbett et al., (2014) and Wehner et al., (2015) and ash bed data from Deluca (2016) for generating a robust, regional correlation of Boquillas/Eagle Ford Group-equivalent strata across west Texas. This approach refines spatial resolution of paleogeographic reconstructions while temporally constraining stratal surfaces and isotopic events on regional scales.

The Boquillas Formation outcrops have variable thicknesses over relatively short distances (Cooper and Cooper, 2014; Cooper et al., 2008; Donovan et al., 2015; Donovan and Staerker, 2010; Miller, 1990) and contains strata deposited within storm wave base as indicated by hummocky cross-stratification (HCS; Donovan et al., 2012; Gardner et al., 2013; Miller, 1990; Wehner et al., 2015). The Boquillas Formation has biostratigraphic

markers constraining its age in BBNP (Cobban et al., 2008; Cooper et al., 2005; Cooper and Cooper, 2014), but those markers are not yet supported with other dating techniques. Identification of inoceramids recovered at Ernst Tinaja is difficult, as most Cretaceous Western Interior Seaway (KWIS) inoceramid experts are retired or deceased. Bentonite age determinations in the Boquillas Formation in BBNP serve to temporally constrain diachroneity of depositional sequences while serving as an anchor for quantification of sedimentation rates in the resulting temporally-defined stratigraphic intervals. Data from the Ojinaga Formation (Mule Canyon) and Eagle Ford Group (Lozier Canyon), in conjunction with limited data from strata partially equivalent to the Ernst Member in Mexico (Indidura Formation), Jeff Davis (Chispa Summit Formation) and El Paso (Boquillas Formation) counties provides information critical for building a chronostratigraphic framework which integrates outcrop and subsurface data in regional Cenomanian–Turonian studies of the KWIS.

Obtaining temporally-precise ages of bentonites near unconformities constrains timing of stratal surface development and isotopic events while providing critical data for determining sedimentation rates and identifying disconformities in stratigraphic section. This study integrates CA-IDTIMS U-Pb dating methods with biostratigraphic (foraminifera, calcareous nannofossils, ammonites and inoceramid bivalves), lithostratigraphic (sedimentary structures and lithologies) and chemostratigraphic ($\delta^{13}C_{carb}$ stable isotopes, HHSGR and HHXRF) data proxies within the Ernst Member in BBNP to build a high-resolution chronostratigraphic framework of regionally-correlative stratal

surfaces, isotopic and biostratigraphic events between west and south Texas, Mexico and New Mexico.

2. GEOLOGIC SETTING

2.1 The Late Cretaceous Western Interior Seaway (KWIS)

The Cretaceous Western Interior Seaway (KWIS) developed via flexural subsidence (Kauffman, 1977) facilitated by the Sevier Orogeny, involving the collision of the Farallon and Kula plates with the North American Plate (Shurr et al., 1994) in the Early to Late Cretaceous (~125-105 Ma). Eustatic sea level rise coupled with high ambient air temperatures during the Cenomanian–Turonian resulted in thermal expansion of the oceans and episodic connection and disconnection of the Boreal and Tethys oceans, leading to repeated N-S inundations across the North American mid-continent (Gale et al., 2002; Kauffman and Caldwell, 1994; Kauffman, 1977). These episodic connections and disconnections of the KWIS, a shallow foreland basin during much of the Late Cretaceous (Corbett et al., 2014), partially contributed towards rapid shifts in ammonite diversity and distribution on the San Marcos Platform in Texas (Young, 1986) and microfossil and nannofossil assemblages over geographically large areas (Lundquist, J. personal communication). An updated paleogeographic map spanning the Early-Middle Cenomanian (Figure 2) is based on data from Bilodeau (1986), Corbett and Watkins (2013), DeJong and Addy (Part 1, 2; 1992), Dickinson et al., (1986), Donovan et al., (2016), Donovan and Staerker (2010), Gardner et al., (2013), Hennings (1994), Martini and Ortega-Gutiérrez (2016) and Wilson (1990).

The southern aperture of the KWIS, including most of Texas and northeast Mexico, was subject to numerous recent studies, following the development of the Eagle

Ford unconventional play in central and south Texas (e.g., Denne et al., 2016; Donovan et al., 2012; Donovan and Staerker, 2010; Gardner et al., 2013; Hentz et al., 2014; Hentz and Ruppel, 2010; Tian et al., 2013). Improving temporal constraints on biostratigraphic proxies in Eagle Ford-equivalent strata, including Lower Eagle Ford (LEF)- and Upper Eagle Ford (UEF)-equivalent strata in west Texas, New Mexico and Mexico can be achieved by age-dating and correlation of some of the >200 volcanic events of the Late Cretaceous, which deposited ash beds across the KWIS (Elder, 1988; Kauffman, 1977). Although the timing of these volcanic events is not well understood (Elder, 1988; Kauffman, 1977), the source of ash beds in west Texas may be the Blue Mountains of central and northeast Oregon, which have migrated more than 1300 km northward from their position prior to the Laramide Orogeny (see Hildebrand, 2015). Ash plumes would have pushed E-W or WSW-ENE from the Blue Mountains by paleowind currents during the Cenomanian–Turonian (see Elder, 1988; Slingerland et al., 1996, Figure 5). Other ash plumes, including the laterally-correlative A, B, C, D and X bentonites characterized in Pueblo, Colorado can be correlated into central New Mexico, Colorado, north (Elder, 1988; Kennedy et al., 2000) and south Texas (Eldrett et al., 2015).

Regional-scale lateral continuity of cyclic Cretaceous strata within the KWIS led to extensive study of cyclic controls on its deposition (e.g., Gale et al., 2002; Gilbert 1895; Grosskopf, 2015; Hinnov, 2013; Kauffman and Caldwell, 1994; Kauffman, 1977; Meyers et al., 2012; Meyers et al., 2001; Molenaar, 1983; Sageman et al., 1997). Aside from identification of cycles within the KWIS, some were correlated across the entire seaway to better understand the role of Milankovitch-forcing on the deposition of sediments

during the Late Cretaceous (Grosskopf, 2015; Hinnov, 2013; Sageman et al., 1998). Globally-correlative marine incursion events operated on 7-10 Ma cycles, corresponding with the 3rd-order cyclicity (Haq et al., 1987; Haq, 2014) and for the Eagle Ford Group, specifically (Lowery et al., 2014). Delineating Milankovitch-forcing on depositional cycles where timescales have significant uncertainty is difficult (Park and Herbert, 1987). Additionally, many Western Interior studies fail to identify timescales used in their analysis (e.g., Geologic Time Scale (GTS) 2004 (Ogg et al., 2004) versus GTS 2012 (Gradstein et al., 2012)). Thus, these analyses use temporally-sensitive data from more than one timescale and amalgamate temporally-inequivalent datasets.

2.2 Big Bend National Park (BBNP)

Big Bend National Park records three major tectonic events, including the 1) Late Paleozoic Marathon-Ouachita Orogeny, 2) Early Cretaceous Sevier Orogeny and 3) Late Cretaceous Laramide Orogeny, followed by Neogene-Recent Basin and Range extension (Haenggi, 2002). Early Late Cretaceous Boquillas sedimentation in BBNP was subjected to differential subsidence and/or cementation, followed by uplift (Miller, 1990) and/or deposition on the spatially and temporally irregular, disconformable surface at the top of the Buda Limestone (Donovan et al., 2016).

2.2.1 Boquillas Formation

The Boquillas Formation, first identified as the Boquillas Flags by Udden (1907), was deposited unconformably above the Buda Limestone, a unit consisting mostly of skeletal wackestone and mudstone and whose uppermost 2.6 m (8.5 ft) preserves evidence for subaerial exposure in Big Bend (Tiedemann, 2010; Lock et al., 2007) and northern

Coahuila, Mexico (Powell, 1965). Boquillas Formation deposition occurred during a marine transgression at the base of the Zuni Supersequence of Sloss (1963). Deposition of the Boquillas Formation was contemporaneous with active volcanism during the Late Cretaceous (Befus et al., 2008; Desmares et al., 2007), resulting in a high concentration of volcanic events recorded in the Lower Eagle Ford equivalents (see Donovan and Staerker, 2010; Deluca, 2016) and Boquillas Formation at BBNP. The Boquillas Formation is comprised of two members: the lower Ernst Member and upper San Vicente Member. The San Vicente Member is laterally equivalent to the Austin Chalk (Maxwell et al., 1967) and Taylor Group of south and central Texas (c.f. Cooper and Cooper, 2014a; 2014b, 2014). The contact between the Ernst and San Vicente members was recently revised to coincide with the base of the *Allocrioceras hazzardi Zone* (Cooper et al., 2005).

2.2.1.1 Ernst Member

The type section for the Ernst Member of the Boquillas Formation is at Ernst Tinaja, a canyon incised through Cuesta Carlota and comprised of W- and WSW-dipping Cretaceous strata trending NNW-SSE within BBNP, Brewster County, Texas (Ferrill et al., 2016; Maxwell et al., 1967, Moustafa, 1988). Cuesta Carlota forms the western flank of Sierra del Carmen, a mountain range formed by northeast-directed contraction during the Laramide Orogeny (Ferrill et al., 2016; Moustafa, 1988) and southwest-directed Basin and Range extension (Maxwell et al., 1967). Ernst Tinaja records lamina- to bed-scale thrust faulting that produced hanging wall anticlines, folds and discordant stratal relationships with offsets ranging from 0.5-9 cm (Ferrill et al., 2016).

The Ernst Member is partially laterally equivalent to the Eagle Ford Group and Austin Chalk of south, central and north Texas (Figure 3), the Chispa Summit Formation of Jeff Davis and Hudspeth counties (Kennedy et al., 1989; Adkins, 1933; King and Adkins, 1946; Passagno, 1967; 1969), the Ojinaga (Frush and Eicher, 1975; Moore, 2016; Wolleben, 1968; Flores, 2013), Indidura (Duque-Botero et al., 2008) and Agua Nueva (Goldhammer and Johnson, 2001; Winker and Buffler, 1988; Seibertz, 1998) formations of Mexico, the Greenhorn Formation of CO, NM and OK (Kennedy et al., 2000) and Mancos Shale of AZ, CO, NM, UT and WY (Passagno, 1969). The Ernst Member also is approximately equivalent to the Boquillas Flags of Udden (1907; Maxwell et al., 1967), the Rock Pen and Langtry members of Passagno (1969) and the "Pinch and Swell," "Flaggy," "Ledgy," and "Laminated" units of Freeman (1968).

The basal 5–7 m (16–23 ft) of the Ernst Member, equivalent to the "Pinch and Swell" unit of Freeman (1968), is composed of calcareous mudstone intercalated with skeletal (foraminiferal) peloidal packstone/grainstone (Tiedemann, 2010) and abundant, often indurated, bentonites 1-25 mm thick. Stratigraphically above this layer (renamed by Denne et al., (2016) as the 'Terrell Member'), the Ernst Member transitions into dark grey, organic-rich calcareous mudstone interbedded with 3–7 cm thick skeletal wackestone/packstone beds. Further up section bentonites are frequent, ranging in thickness between 3–50 mm, and occur between light grey, organic-rich, calcareous mudstone, skeletal wackestone/packstone (with inoceramids and other bivalves) and organic-rich, black shale. The first ~30–40 m (98–131 ft) of Ernst Member strata have colorful Leisegang banding (e.g., red, purple, orange, yellow). Immediately above this

interval, the Ernst Member gradually transitions into laminated calcareous shale with weathered pyrite nodules interbedded with skeletal wackestone/packstone beds 4–11 cm thick. Bentonites in this interval have thicknesses approaching 150 mm, are poorly-indurated and may be nodular in appearance (intracarbonate ash nodules). The uppermost 30–40 m (98–131 ft) of the Ernst Member is dominated by a lesser abundance of laminated calcareous shale interbedded with increasing abundance and thickness (up to 20 cm) of Fe-rich (and occasionally organic-rich) skeletal wackestone/packstone beds. The top of the Ernst Member is defined here as the base of the *Allocrioceras hazzardi* (Young) Zone (AHZ), which contains the inoceramid *Cremnoceramus deformis erectus* of the Early Coniacian (Cobban et al., 2008; Cooper et al., 2008; Cooper et al., 2005; Cooper and Cooper, 2014). At the study sections within BBNP (especially Ernst Tinaja; Figure 1, 3), the lithological shift from shale-prone to limestone-prone strata occurs ~70.1 m (230 ft) above the base of the Ernst Member, above which limestone beds occur more often and with increased average thickness (approaching ~45 cm), and are separated by thin intervals (averaging < 30 cm) of laminated, calcareous shale.

Although revised stratigraphic interpretations of the Boquillas Formation were completed recently (Donovan et al., 2015, Donovan and Staerker, 2010), precise ages of strata within the Ernst Member, especially within BBNP, were not quantified by U-Pb dating. Ash bed ages were reported for the Buda Limestone/Boquillas Formation (96.8+1.2/-0.7 Ma) and Upper Boquillas/Austin Chalk (87.13 ± 0.3 Ma) contacts exposed by road cuts in Val Verde and Terrell counties (Pierce, 2014). However, these Induction Coupled Plasma-Mass Spectrometry (ICP-MS) U-Pb ages are of insufficient resolution to

build a high-resolution chronostratigraphic framework of regionally-correlative stratigraphic surfaces, biozones and isotopic events. Depositional age estimates of the Ernst Member were previously dependent on the biostratigraphic control provided by various ammonite zones, ranging from Early Cenomanian–Coniacian (Cobban et al., 2008; Cooper and Cooper, 2014; Denne et al., 2014). A basic comparison of strata time-equivalent to the Boquillas Formation in west Texas is shown in Figure 3. One interval within Eagle Ford-equivalent strata, the Oceanic Anoxic Event 2 (OAE2), records a globally-correlative period of oceanic anoxia spanning the C/T boundary (Phelps et al., 2015; Elrick et al., 2009, Sageman et al., 2006) and is contemporaneous with volcanism from Large Igneous Provinces (LIPs) in Madagascar, the Caribbean and the Ontong-Java submarine plateaus (Elrick et al., 2009; Kuroda et al., 2007; Sinton and Duncan, 1997; Turgeon and Creaser, 2008). OAE2 was an event which spanned 400-800 kyr (710 kyr in Lozier Canyon; Deluca, 2016). The Ojinaga Formation section at Mule Canyon, Quitman Mountains, according to new calcareous nannofossil data, does not record the C/T boundary (Moore, 2016).

2.2.1.2 Biostratigraphy of the Ernst Member (and equivalents)

The biostratigraphy of the Ernst Member and its lateral equivalents is well-defined by ammonite and inoceramid zonation (Cobban et al., 2008; Frush and Eicher, 1975; Maxwell et al., 1967). Though these zones can be temporally constrained on local scales by dating bentonites, this doesn't preclude the challenge of quantifying the time-transgressive lateral extension of biozones on regional scales. Additionally, regional age correlations of biozones can be complex due to discrepancies between faunal

nomenclature referenced in literature, e.g. *Moremanoceras elgini*, formerly *Desmoceras (Pseudouhligella) elgini* (Young) (Cobban et al., 2008; Daugherty and Powell, 1963).

Euhystrichoceras adkinsi occurs in the basal 0.2–1 m (0.6–3.3 ft) of the Ernst Member in Pico Etereo (~15.5 km ENE of Ernst Tinaja, BBNP; Powell, 1965), the basal 0.4 m (1.3 ft) of the Ernst Member in Ernst Tinaja (Cobban et al., 2008), and ~9.2 m (30 ft) above the basal Ojinaga Formation in the *Acompsoceras inconstans* Biozone (Cobban et al., 1989) at Mule Canyon (Cobban and Hook, 1980; 1989) where a distinctive, limestone bed ~20 cm thick occurs (Kennedy et al., 1989). The Early Cenomanian *Acompsoceras inconstans* Biozone also is correlative with the basal 0.9 m (3 ft) of the Chispa Summit Formation (Adkins, 1932; Cobban and Hook, 1980; Kennedy et al., 1989; Orth, 1993) and basal 1 m (3.3 ft) of the Ernst Member at Hot Springs, BBNP (Cobban et al., 2008; Cooper and Cooper, 2014; Wehner et al., 2015). Middle Cenomanian fauna, including *Inoceramus arvanus* Stephenson of the *Acanthoceras bellense* Zone, were recovered 3.0 m (10 ft) above the base of the Ernst Member at Ernst Tinaja, 4.8 m (15.8 ft), 1.8 m (5.9 ft) , and 2–4 m (6.6–13.1 ft) above the base of the Chispa Summit Formation at the town of Chispa (Jeff Davis County), the Eagle Mountains and Gold Hill, respectively, ~5–6 m (16.4–19.7 ft) at Hot Springs in BBNP (Frush and Eicher, 1975) and at the basal limestone bed marking the base of the Ernst Member at Cerro de Cristo Rey, El Paso, Texas (Cobban et al., 2008). Late Cenomanian fauna such as *Inoceramus pictus* occurs at Hot Springs, ~12 m (39 ft) and 21–22 m (69–72 ft) above the basal contact (Cooper and Cooper, 2014) and at Chispa, Texas in the *Neocardioceras juddii* Biozone,

~39.5 m (130 ft) above the base of the Chispa Summit Formation, just beneath the C/T boundary (Kennedy et al., 1989).

Foraminiferal studies conducted within the first meter of the Ernst Member at Dagger Flat, ~36 km NNW of Ernst Tinaja in BBNP (Tiedemann, 2010) and throughout the Ernst Member within 'globigerinid argillaceous wackestone' at Ernst Tinaja (Frébourg et al., 2016) suggest low benthic (<5-10%) relative to planktonic (~90-95%) foraminiferal abundances. Publicly-available calcareous nannofossil data is sparse throughout west Texas and is largely absent in Cenomanian-Turonian studies of northeast Mexico.

3. METHODS

A measured section of the Ernst Member type section at Ernst Tinaja was constructed as one, continuous segment traversing from 235-260 azimuth (SW to WSW; Figure 4). A Jacob's Staff and Brunton Compass were used to measure 1.56 meter increments in the section. Lithostratigraphic measurements were made in 15 cm intervals, while hand samples for chemostratigraphic analysis were collected in ~46 cm (1.5 ft) intervals. Additional samples for calcareous nannofossil and foraminiferal biostratigraphy were collected, on average, in 3.0 m (10 ft) increments. Outcrop photography was performed to photo-document the Ernst Member type section at Ernst Tinaja. Strike and dip measurements (with position data) were taken every 10 m of section (see Appendix C).

The CA-IDTIMS method was used to analyze zircons for $^{238}U/^{206}Pb$ content from ash beds (see Appendix C). HHSGR measurements were taken by Terraplus RS-230 scintillometers from -1.5 m (-5 ft) to 93.3 m (306 ft) in 0.3 m (1 ft) increments. In total, 159 slabbed hand samples (collected at Ernst Tinaja) were analyzed by Matthew Wehner for trace element composition using the Thermo Scientific Niton XL3t GOLDD+ X-Ray Fluorescence analyzer, utilizing calibrations developed by Harry Rowe (University of Texas: Austin). Slabbed samples were sampled (~1.5 g) for stable isotopic analyses ($\delta^{13}C_{carb}$ and $\delta^{18}O_{carb}$). Calcareous nannoplankton and foraminiferal analyses were conducted by Atlantes Geoconsulting, Inc. (Scott Staerker) and Jason Lundquist, respectively.

3.1 Sedimentation Rates

Bentonite ages (isochrons) determined by Deluca (2016) and Peavey (this paper) were projected into all west Texas sections (see Section 4.5) in agreement with data analyzed from chemostratigraphic and biostratigraphic proxies. Correlation (COR) of isochrons into all four west Texas localities (Mule Canyon, Hot Springs, Ernst Tinaja and Lozier Canyon) enabled the calculation of sedimentation rates of the measured section at Ernst Tinaja. COR-derived sedimentation rates were calculated by dividing the total thickness of each spatial (thickness) interval by the maximum, minimum, and average CA-IDTIMS-derived time intervals.

3.2 Methods of Regional Correlation

Spatial constraints for this chronostratigraphic framework include all chemostratigraphic (HHSGR, HHXRF, stable isotopes) and lithostratigraphic data. Temporal constraints for this framework include all biostratigraphic proxies (ammonites, inoceramids, calcareous nannofossils and foraminifera) and CA-IDTIMS-derived bentonite ages. Correlation of surfaces was achieved by verifying the agreement between spatial and temporal constraints and the spatial and temporal position of surface picks before integration into the chronostratigraphic framework.

4. RESULTS

This study presents three CA-IDTIMS $^{238}U/^{206}Pb$ zircon ages for ash samples in the Ernst Member at Ernst Tinaja, each of which has a 2σ error ≤0.2% (Sampled Bentonite Summaries, Table 1). A single detrital age (~305 Ma; Brent V. Miller) from a nodular, intracarbonate ash bed located approximately 64 m (210 ft) above the base of the Ernst Member (Austin Chalk-equivalent) at Hot Springs also was determined. These ages are incorporated into a regional chronostratigraphic framework supported by 38 calcareous nannofossil (Calcareous Nannofossils in the Ernst Member at Ernst Tinaja, Table 2) and 10 foraminiferal (Foraminifera in the Ernst Member at Ernst Tinaja, Table 3) analyses and ammonites and inoceramids (Cobban et al., 2008; Cobban and Hook, 1980; Cooper and Cooper, 2014; Kennedy et al., 1989; Maxwell et al., 1967; Young, 1986b) for biostratigraphic control. Improved robustness of correlation is achieved using a suite of 46 $\delta^{13}C_{carb}$ and 159 HHXRF analyses in conjunction with HHSGR data, isochron ties and stratal surfaces (sequence boundaries (SBs), transgressive surfaces (TSs) and maximum flooding surfaces (MFSs)) between west Texas outcrops (Figure 5).

4.1 Lithostratigraphy and Sedimentary Structures

A stratigraphic column for the Ernst Member type section at Ernst Tinaja (Figure 5) was measured and is 84.6 m (277.5 ft) thick. At Hot Springs, the stratigraphic thickness of the Ernst Member is 85 m (279 ft). At Ernst Tinaja, the lower 52.7 m (173 ft) of Ernst Member strata is Eagle Ford Group-equivalent and the upper 31.9 m (104.5 ft) from 52.7-84.6 m (173–277.5 ft) is equivalent to the lower part of the Austin Chalk. Swaley Cross

Stratification (SCS) and HCS, including HCS/SCS composite beds, ripple laminae and wavy bedding are dominant sedimentary structures in the basal 7.7 m (25 ft) but persist in the lowest 27.4 m (90 ft) of the section (Figure 6). Some folded bedding is attributed to structural deformation, induced by Laramide-associated thrusting. Diagenetic alteration and Leisegang banding occurs locally, likely facilitated by inundation of hydrothermal fluids associated with Eocene-Oligocene rifting and extension in west Texas (c.f. Maxwell et al., 1967). Carbonate mudstone beds at 16 m (53.6 ft), 19.8 m (65 ft) and 21.3 m (70 ft) have abundant *Chondrites* trace fossils and these become less common above 52.7 m (173 ft, Figure 5; Figure 6). HCS occurs at ~28 m (92 ft) above a nodular, cemented, burrowed foraminiferal wackestone/packstone at 27.4 m (90 ft), which has burrows ~1 cm wide, ≤ 3.5 cm deep filled with indurated ash. Bed 27.4 m (90 ft) was deposited between two bentonites at 27.3 m (89.5 ft) and 27.6 m (90.5 ft), respectively (Figure 6). Nodular, intracarbonate ash beds occur at 33.5 m (110 ft), 47.2 m (155 ft) and 50.3 m (165 ft) and co-occur with Fe-oxide nodules oriented sub-parallel with respect to bedding. Soft sediment deformation in carbonate wackestone/packstone beds is prominent near 25.6 m (84 ft), 41.8 m (137 ft), and 52.1 m (171 ft). Bioturbation in skeletal packstone beds occurs from 52.4–53 m (172–174 ft). *Chondrites* traces cover tops of carbonate beds at 50.9 m (167 ft), 52.1 m (171 ft) and 54.6 m (179 ft), respectively. The Eagle Ford Group/Austin Chalk-equivalent contact is located stratigraphically at ~52.7 m (173 ft), and skeletal packstone/grainstone beds within 1 m (3.3 ft) above or below the contact are wavy, nodular and have HCS. Burrows co-occur with weathered pyrite nodules at 56.4 m (185 ft). Laminated bedding dominates the section above 64 m (210 ft), coincident with thick

successions of fissile, calcareous shale which becomes friable with increased clay content from 64–73.2 m (210–240 ft). One nodular, intracarbonate ash bed occurs at 78.6 m (258 ft), but was not collected. HCS and weathered pyrite nodules co-occur with the ammonite *A. hazzardi* and inoceramid *C. deformis erectus* at 84.6–86.5 m (277.5–284 ft). Discrepancies in the quality of outcrop exposures between Ernst Tinaja and Hot Springs in the Big Bend area preclude accurate determination of lateral variability.

4.2 CA-IDTIMS

Bentonites (21 in total) were collected at three sites, including the Ojinaga Formation at Mule Canyon, Quitman Mountains (4), and the Boquillas Formation at Hot Springs (6) and Ernst Tinaja (11) in BBNP. Of these, four ash beds from Hot Springs and three ash beds from Ernst Tinaja were processed, six of which contained abundant zircons. Sample (HS-BOQ-4) was rejected from analysis due to insufficient zircon abundance. Of the remaining six samples, one (HS-BOQ-51.00 m) was determined to be detrital, as zircon ages were uppermost Pennsylvanian (~305 Ma; Brent V. Miller, personal communication). Descriptions and ages of zircons recovered from bentonite samples are presented in Table 1. Processed bentonites were collected 0.3 m (0.9 ft), 7.55 m (24.6 ft) and 52.05 m (170.8 ft) above the base of the Ernst Member at Ernst Tinaja and 0.1 m (0.3 ft), 4.55 m (14.9 ft) and 62.5 m (205 ft) above the base of the Ernst Member at Hot Springs. Ages for bentonites processed from the Ernst Member type section at Ernst Tinaja, BBNP are: 1) 97.49 ± 0.12 Ma at 0.3 m (0.9 ft), 2) 95.99 ± 0.15 Ma at 7.5 m (24.6 ft) and 3) 91.16 ± 0.16 Ma at 52.1 m (171 ft) above the Buda Limestone/Ernst Member contact.

4.3 Calcareous Nannofossil and Foraminiferal Biostratigraphy

All calcareous nannofossil and foraminiferal data, and ammonite and inoceramid biostratigraphy from literature were temporally calibrated to the Geologic Time Scale 2012 (Gradstein et al., 2012). In total, 38 biostrat/paleo samples were collected between 3.0–97.5 m (10–320 ft). Nannofossil abundance scans were performed on all 38 paleo samples, with 22 of those undergoing detailed analyses (Table 2). Detailed foraminiferal scans were performed on 10 of the 38 paleo samples (Table 3).

4.4 Chemostratigraphy

The spectral gamma ray curve (Figure 5) is composed of 311 measurements (made at 0.3 m (1 ft) increments) and trace element concentration curves constructed by 159 measurements made at 0.4 m (1.5 ft) increments. A plot of the decoupled spectral gamma ray curve (Figure 7) compliments chemostratigraphic data from U, Mo and V (proxies for anoxia; Alego and Rowe, 2012; c.f. Tribovillard et al., 2006) Zr and Ti, (siliciclastic input proxies; Tribovillard et al., 2006, Turner et al., 2015) Sr and Ca (carbonate proxies; Banner, 1995; Turner et al., 2015), Al and K (for clay minerals/feldspars; Tribovillard et al., 2006; c.f. Sageman and Lyons, 2004) and Si and Si/Ti ratios for quartz in section (c.f. Pearce and Jarvis, 1992; Pearce et al., 1999; Tribovillard et al., 2006; Turner et al., 2015; Figure 8). For all other plots, including raw data, see Appendix C. A plot of redox conditions for the LEF-, UEF- and Austin Chalk-equivalents in the Ernst Member and the AHZ (at the base of the San Vicente) at Ernst Tinaja is presented in Figure 9 (c.f. Eldrett et al., 2014).

Forty-six slabbed, whole-rock samples were processed and analyzed for $\delta^{13}C_{carb}$ stable isotopes (see Figure 5). Roughly half of the sampling for stable isotopic analyses

was between 24.4–38.1 m (80–125 ft) to identify CIEs indicative of OAE2, and remaining samples chosen at ~3.0 m (10 ft) increments throughout the section. Shifts of >2 ‰ $_{VPDB}$ in $\delta^{13}C_{carb}$ occur between ~3.3–5.5 m (11–18 ft) and between 27.4–33.0 m (90–108 ft).

4.5 Sedimentation Rates

Sedimentation rate estimates for the Ernst Member type section are presented in Table 4 (Sedimentation Rates for west Texas Localities). Minimum, maximum and averaged sedimentation rates were generated according to correlation of isochrons and biostratigraphic events between Lozier Canyon and Ernst Tinaja (Figure 10). Correlation (COR)-derived MAX and MIN sedimentation rates were not calculated from 0.3–1.5 m (1.0–5.0 ft) and 7.5–16.1 m (24.7–52.7 ft), due to overlap in uncertainties from CA-IDTIMS-dated bentonites. The only biostratigraphic event used for analysis was the age range of the *H. helvetica* Zone (Tiedemann, 2010), which temporally defines the upper boundary of 22.4–27.3 m (73.4–89.5 ft) and the lower boundary of 27.3–47.5 m (89.5–155.7 ft).

4.6 Chronostratigraphy

Chronostratigraphic charts were generated for Ernst Tinaja (Figure 11) and tied to other west Texas localities (Figure 12) in an attempt to quantify temporal variation in deposition of Eagle Ford Group-equivalent strata in west Texas. These charts are supported by nannofossil, foraminiferal and ammonite biostratigraphy and CA-IDTIMS-dated bentonites, but are not generally paired with stratal surfaces.

The local chronostratigraphic chart for the Ernst Member Type Section at Ernst Tinaja (Figure 11) spans ~7.7 myr and records ~5.5 +0.6/-1.1 myr of deposition. The

sediments preserved at the basal 2.4–3.0 m (8-10 ft) of the Ernst Member are Early Cenomanian, verified below by a bentonite age (97.49 ± 0.12 Ma) 0.3 m (0.9 ft) above the Buda Limestone/Ernst Member contact and the occurrence of Early Cenomanian ammonites *Moremanoceras bravoense* Cobban and Kennedy and *Euhystrichoceras adkinsi* (Powell) collected ~0.5 m (1.5 ft) above the base at Ernst Tinaja (Cooper et al., 2008). At 3.0 m (10 ft) the Middle Cenomanian inoceramid *Inoceramus* arvanus of the *Acanthoceras bellense* Zone (Cooper et al., 2008; Cobban et al., 2008) occurs. Specimens of *Ostrea beloiti* of the Middle Cenomanian *Acanthoceras amphibolum* Zone, *R. cushmani? and R. asper* were recovered approximately 4.9 m (16 ft) above the base of the Ernst Member (Cooper et al., 2008).

5. DISCUSSION

The Ernst Member of the Boquillas Formation in BBNP is laterally-equivalent to the Eagle Ford Group from 0–52.7 m (0–173 ft) and above this point becomes laterally-equivalent to the Austin Chalk to the top of the Ernst Member (52.7–84.6 m; 173–277.5 ft). At 84.6 m (277.5 ft), the Ernst Member reaches the base of the AHZ, corresponding to the base of the overlying San Vicente Member of the Boquillas Formation. This boundary zone occurs within the earliest Coniacian (Cooper et al., 2005).

5.1 Chronostratigraphy and Biostratigraphy

The hiatus straddling the Buda Limestone/Ernst Member contact is < 1 myr in duration, constrained above by a bentonite age (97.49 ± 0.12 Ma) and below by an occurrence of *Neophlycticeras (Budaiceras) hyatti* < 1.6 m (5 ft) below the Buda Limestone/Ernst Member contact at Hot Springs (~ 98.5 Ma; Cobban et al., 2008). A few specimens of *R. cushmani?* and a single *R. asper* nannofossil suggest 4.9 m (16 ft) to be latest Middle or earliest Late Cenomanian (just above the occurrence of the Mid-Cenomanian event preserved at Ernst Tinaja). These biostratigraphic proxies and bentonite age, when considered simultaneously, suggest the occurrence of a condensed section with up to 500-600 kyr duration between 0.5–3.0 m (1.5–10 ft), in agreement with a bentonite age of 97.49 ± 0.12 Ma from the basal 0.3 m (0.9 ft) in BBNP. This finding is supported by the region-wide development of a Middle Cenomanian disconformity across the Gulf of Mexico plain associated with coeval relative sea level drop (see Haq, 2014) and uplift along the northern rim of the Gulf of Mexico (Ewing, 2013; Sohl et al., 1991;

Anderson, 1979). Chemostratigraphic data from the Ernst Member at Ernst Tinaja distinguish chemofacies between 0–4.6 m (0–15 ft) distinct from strata above or below, where major shifts in Ti, Zr, Sr, Ca, U, Mo and V occur. U, Mo, Ca, Ti, Zr and Si/Ti spike within this interval, just below a peak in Sr at ~2.1 m (7 ft). A surface immediately above the Sr spike at ~2.1-2.4 m (7-8 ft) is interpreted as a condensed section and is located ~2.4 m (~8 ft) above the Buda Limestone/Ernst Member contact. Extension of this condensed section into Lozier Canyon is supported by nannofossil, foraminiferal and ammonite biostratigraphy, as well as a CA-IDTIMS-dated bentonite age (97.14 ± 0.36 Ma) and similar chemostratigraphic signature to the flooding surface in the basal 0.3 m (1 ft) at Lozier Canyon.

The bed at 27.4 m (90 ft, Figure 6) marks the disconformable surface between LEF/UEF-equivalent strata in the Ernst Member at Ernst Tinaja, representing ~0.8–1.3 myr of missing time. The duration of this hiatus is supported by foraminiferal, ammonite and nannofossil biostratigraphy and the absence of the OAE2 positive CIE which has a duration of ~710 kyr in Lozier Canyon (Deluca, 2016), and is coincident with the K65 sequence boundary (SB) of Donovan et al. (2012). A hiatus of comparable duration at Lozier Canyon is associated with the development of the K70 SB, which occurs and cannibalizes sediment at Lozier Canyon, likely removing the C/T boundary at that locality (Donovan et al., 2016).

Continued occurrence of *C. kennedyi*, *R. asper* and *H. chiastia* through 29.8 m (97.8 ft) in the Ernst Member suggest these strata are Late Cenomanian, although the planktonic foraminiferal assemblage *H. Helvetica, P. stephani and D. hagni* from the same

sampled horizon suggest latest Early Turonian deposition. Disagreement between microfossil and nannofossil interpretations, coupled with an occurrence of HCS stratigraphically at 28.4 m (92 ft) may suggest significant reworking of nannofossils stratigraphically above the LEF/UEF hiatus.

Nannofossil and foraminiferal biostratigraphy indicates the interval 27.4–33 m (90–108 ft) is latest Early Turonian, the interval 37.5–42.7 m (123–140 ft) is Middle Turonian, and the interval 42.7–84.6 m (140–277.5 ft) is Late Turonian. The hiatus located at the Eagle Ford Group/Austin Chalk-equivalent boundary at Lozier Canyon correlates to nodular, skeletal packstone/grainstone beds (containing HCS) at 52.4 m (172 ft) and 53 m (174 ft) in the Ernst Member at Ernst Tinaja, BBNP. This hiatus is expected to be of smaller duration than was originally proposed (see Donovan et al., 2012). Between 52.7–69.5 m (173–230 ft) is regarded as a Late Turonian, Austin Chalk-equivalent section preserved only in the Maverick Basin (Scott Staerker, personal communication; in adherence to GTS 2004 (Ogg et al., 2004)) especially considering the ~32 m (105 ft) of Late Turonian, Austin Chalk-equivalent deposition spanning 52.7–84.6 m (173–277.5 ft) at BBNP, and the revision of the physical boundary (Cooper et al., 2005) and temporal boundary (Gradstein et al., 2012) of the earliest Coniacian in the southern KWIS. The Ernst Member/San Vicente Member boundary occurs at 84.6 m (277.5 ft), where the ammonite *Allocrioceras hazzardi* co-occurs with the earliest Coniacian inoceramid *Cremnoceramus deformis erectus* (Cooper et al., 2005; Cooper and Cooper, 2014a; 2014b). Strata above 84.6 m (277.5 ft) are interpreted as Early Coniacian, and are included in the San Vicente Member of the Boquillas Formation.

5.2 Depositional Environments and Redox Conditions

Lithostratigraphy, sedimentary structures and foraminiferal biostratigraphy were integrated with $\delta^{13}C_{carb}$ data to determine depositional environments within the Ernst Member at Ernst Tinaja. Chemofacies were employed to support depositional environment interpretations, and are defined by rapid, coeval shifts in multiple trace element proxies above and/or below target boundaries (e.g., unconformities or stratal surfaces laterally-correlative to Eagle Ford Group- and Austin Chalk-equivalents of south and central Texas (Deluca, 2016; Donovan et al., 2017; Donovan et al., 2016; Donovan et al., 2012).

5.2.1 Eagle Ford-equivalent Section of the Ernst Member

Storm beds, including HCS and SCS are most abundant in the lowest 27.4 m (90 ft) of the Ernst Member at Ernst Tinaja and suggest depositional environments commonly within storm wave base during LEF-equivalent deposition. The basal 4.6 m (15 ft) of section preserves a geochemical signature characterized by relatively low concentrations of Ti, Zr and K, suggesting low siliciclastic influence on deposition. Moderate levels of U and Mo persist 0–3.0 m (0–10 ft), but reach nearly zero between 3.0–4.6 m (10–15 ft), suggesting a significant drop in TOC and increase in oxic conditions, concomitant with increased HCS. A 6-7% benthic foraminiferal population recovered at 3.0 m (10 ft) also is consistent with this interpretation. A part of the CIE associated with the Mid-Cenomanian Event is preserved between 3.3–5.5 m (11–18 ft) at Ernst Tinaja and Hot Springs, and is ~ +2 ‰.

The interval between 4.6–27.4 m (15–90 ft) preserves high concentrations of U, Mo, and V, suggesting 1) highly reducing conditions and 2) high TOC. The disconformity at 27.4 m (90 ft) is defined lithostratigraphically and by a +2.4 ‰ shift in $\delta^{13}C_{carb}$ between 27.3 m (89.5 ft) and 27.6 m (90.5 ft). HCS occurs immediately above the LEF/UEF disconformity (at 27.4 m; 90 ft) at 27.8 m (92 ft) and may suggest stratigraphic reworking spanning 27.4–33 m (90–108 ft), where Late Cenomanian nannofossils were recovered from the same sample as a latest Early Turonian planktic foraminifer assemblage at 29.8 m (97.8 ft).

The absence of HCS/SCS from 37.5–42.7 m (123–140 ft), coupled with a foraminiferal assemblage containing only 1-2% benthic foraminifera, a single occurrence of *Chondrites* and low levels of U and Mo and moderate levels of V may suggest 1) deposition in relatively oxic waters and 2) moderate levels of TOC. Ripple cross laminae, wavy bedding and an abundance of pyrite nodules from 42.7–52.7 m (140–173 ft) suggest deposition above storm wave base and short periods of time when palaeoceanographic conditions were favorable for pyrite formation. A foraminiferal sample collected near the top of the interval at ~53 m (~174 ft) contained no benthic foraminifera.

Low benthic foraminiferal abundances may be accounted for by 1) depositional environments above storm wave base (Donovan et al., 2012; Wehner et al., 2015), 2) the extension of anoxic and reducing conditions across the southern KWIS (especially during OAEs), or both. Limited data on some CC/UC nannofossil zones determined in the Ernst Member at Hot Springs, BBNP suggest Middle Turonian strata directly overlie Middle Cenomanian strata, and the OAE2 positive CIE and C/T boundary are missing.

5.2.2 Austin Chalk-equivalent Section of the Ernst Member

Between 52.7–84.6 m (173–277.5 ft) in the Ernst Member at Ernst Tinaja, weathered pyrite nodules are rare, bioturbation is absent and HCS/SCS less common than lower in section. However, within 59.4–76.2 m (195–220 ft) and within the AHZ, HCS/SCS, nodular bedding and abundant weathered pyrite nodules occur.

The interval 52.7–84.6 m (173–277.5 ft) is dominated by planar laminae, is more clay- and carbonate-rich (especially from 59.4–76.2 m (195–250 ft), where shale is particularly friable) and is more carbonate prone above 70.1 m (230 ft), where foraminiferal grainstone beds are more frequent, separated by progressively thinner intercalations of laminated, fissile calcareous shale. At 75.1 m (246.5 ft), a foraminiferal sample yielded an assemblage with ~16% benthic foraminifera. Concentrations of U, Mo and V remain relatively low from 52.7–84.6 m (173–277.5 ft) which, when considered with other data proxies, suggests low TOC and a depositional environment which is oxic and more commonly below storm wave base.

The AHZ is characterized chemostratigraphically by relatively large spikes in U, Mo, K and Si, low values of V and Ti and a foraminiferal assemblage (from 86.7 m; 284.5 ft) devoid of benthic foraminifera. An additional foraminiferal sample from 91 m (298.7 ft) yielded ~10% benthic foraminifera. The AHZ was likely deposited above storm wave base, with increased siliciclastic input (from fine quartz sand laminae in the interval). The AHZ represents a shallow water, restricted marine environment (Cooper and Cooper, 2014) and records a euxinic episode in an otherwise oxic depositional environment above storm wave base (c.f. Figure 9).

5.2.3 Redox Conditions of the Ernst Member

LEF-, UEF- and Austin-equivalent Ernst Member and AHZ deposition in BBNP preserve redox signatures indicative of persistent euxinia or dysoxia in the water column and sediments (Figure 9). LEF-equivalent sediments spanning 0–27.4 m (0–90 ft) preserve redox ratio values indicative of persistent euxinia or dysoxia in the water column, and are similar to covariance values elsewhere in the Eagle Ford of south and central Texas (Wehner et al., 2015). UEF-equivalent sediments spanning 27.4–52.7 m (90–173 ft) preserve a shift from LEF-equivalent ratio values, indicating the migration of euxinic or dysoxic zones into the sediments and out of the water column. This trend continues into Austin Chalk-equivalent strata spanning 52.7–84.6 m (173–277.5 ft), where siliciclastic input drives euxinia or dysoxia, which becomes concentrated in sediments (Figure 9). U-Mo covariance charts (e.g., Figure 9) do not provide critical information necessary to identify dominant processes responsible the persistence of euxinic or dysoxic conditions during deposition (Wehner et al., 2015).

5.3 Chronostratigraphic Framework and Facies Model

The integration of litho-, chemo-, bio- and chronostratigraphy offers unique opportunities in overcoming challenges in sequence stratigraphy and basin evolution in petroleum systems, and towards the development of more temporally-defined paleogeographic reconstructions. A chronostratigraphic framework of west Texas, Eagle Ford- and Austin Chalk-equivalent strata is presented in Figure 13. A facies model based on Donovan et al., (2012) was developed and correlated regionally to facilitate a robust, regional-scale temporal and spatial correlation of west Texas outcrops. Additional

information was inferred from global sequence stratigraphy (Haq, 2014) to assign a regional and/or global context to stratal surfaces interpreted for Late Cretaceous deposition in the southern KWIS (Donovan Facies Model, Figure 14).

5.3.1 Stratal Surfaces

Stratal surfaces for figures 13 and 14 adhere to the numbering scheme from Donovan et al., (2012). The interval of the Ernst Member between K63 SB and K63 MFS represents the initial transgression at the start of the Zuni Supersequence of Sloss (1963). The basal 4.6 m (15 ft) of the Ernst Member at BBNP, geochemically distinct from overlying sediments, may only be Eagle Ford-equivalent if the absence of high TOC, U, Mo and V is accounted for by a depositional environment unfavorable for the deposition and/or preservation of organic matter. Alternatively, this interval may represent Maness Shale-, Woodbine Group-, Pepper Shale- and/or False Buda-equivalent deposition, only if the interval was flushed and/or geochemically altered by hydrothermal fluids from Rio Grande rifting (c.f. Maxwell et al., 1967). This interval also occurs in the basal 1.8 m (6 ft) at Lozier Canyon and contains abundant HCS/SCS and multiple deformed beds and debris flow-like beds with clasts >0.3 m (1 ft) in diameter.

An expanded section is preserved between K63 MFS and K64 SB in Lozier Canyon with respect to the BBNP localities, suggesting a condensed section near or within the same interval preserved at BBNP. This interval is ~39 m (128 ft) thick in the Ojinaga Formation at Mule Canyon, but needs to be better constrained temporally (via additional biostratigraphic and bentonite data). This interval is comparable to sub-facies B1-B2 (Donovan et al., 2012).

The K64 sequence is ~4.8 m (15 ft) thicker in BBNP than in Lozier Canyon, and comprises ~150 m (492 ft) of the Ojinaga Formation section at Mule Canyon. This interval is Late Cenomanian, is correlated to sub-facies B3-B5 (Donovan et al., 2012) in Lozier Canyon and is characterized as a bentonite-rich zone (Donovan and Staerker, 2010; Gardner et al., 2013; Hentz and Ruppel, 2010; Hentz et al., 2014; Tian et al., 2013). Late Cenomanian Ernst Member deposits at Ernst Tinaja, corresponding with the top of this interval, record a marine transgression coincident with the maximum inundation of the KWIS (Sohl et al., 1991).

The K65 sequence is composed of Facies C and includes all strata between the K65 and K70 sequence boundaries. Facies C is likely the most stratigraphically-variable facies of the Eagle Ford Group (Davis, 2017), probably due to its connection with peak sea levels in the Phanerozoic (Haq et al., 1987; Haq, 2014) and potential for repeated condensed section or disconformity development (c.f. Cobban et al., 2008). The K65 sequence (Facies C) contains an early interval of Late Cenomanian–earliest Early Turonian strata corresponding to OAE2 at Lozier Canyon, and a late interval of Early Turonian strata which corresponds to the recovery of palaeoceanographic conditions following OAE2 in BBNP. The positive CIE and fossils indicating OAE2 deposition are not preserved in BBNP, even with consideration of composite faunal assemblages suggesting otherwise (Cooper and Cooper, 2014). Temporally inequivalent nannofossil and foraminiferal assemblages from a sample collected at 29.8 m (97.8 ft), HCS/SCS at 28 m (92 ft), three rapid, >2 ‰ shifts in $\delta^{13}C_{carb}$ at 27.7 m (91 ft), 29 m (95 ft) and 31.1 m (102 ft; see Figure 13) and a chemofacies characterized by low U, Mo, V, low-moderate

Zr and Ti, high Ca and increasing Sr (Figure 8; c.f. Turner et al., 2015) in the Ernst Member type section at Ernst Tinaja suggest reworking of, and development of unconformities within, strata between 27.4–33 m (90–108 ft). The K65 sequence was not observed in the Ojinaga Formation at Mule Canyon, except potentially the K65 SB at the top of the section at ~229 m (~750 ft) above the Buda Limestone/Ojinaga Formation contact.

The K70 sequence is regarded as late Middle Turonian–middle Late Turonian, is equivalent to the Langtry Member of the Eagle Ford, and correlates to facies D and E (Donovan et al., 2012). In BBNP, ~6–7 m (20-23 ft) of strata between ~33–39 m (108–128 ft) has a chemostratigraphic signature suggestive of lowstand wedge deposits (c.f. Turner et al., 2015), possibly sourced by material associated with the development of the K70 SB in Lozier Canyon. High global sea levels from 92.6–91.9 Ma (Haq, 2014), coupled with increases in accommodation due to increasing subsidence and/or sediment supply resulted in a preserved accumulation of ~10 m (33 ft) of strata overlying the lowstand wedge deposits below. This interval, between 39–48.8 m (128–160 ft), has a chemofacies with increasing marine signals (e.g., Ca, Sr) and decreasing detrital signals (e.g., Zr, Ti) comparable to transgressive systems tract (TST) deposits (c.f. Turner et al., 2015). As global sea levels began to fall around 91.8 Ma (Haq, 2014), either accommodation decreased in BBNP, or depocenters shifted away from BBNP and towards Lozier Canyon, resulting in an Upper Langtry (E) section preserved in Lozier Canyon ~4 m (13.3 ft) thicker than in BBNP. This interval, between 48.8–52.7 m (~160–173 ft), has 1) a chemofacies with low Mo and V, 2) small increases in detrital signals (Zr, Ti) and 3)

a potential disconformable surface at the Eagle Ford Group/Austin Chalk-equivalent contact, suggesting highstand systems tract (HST) deposits (Turner et al., 2015).

The K72 and K73 sequences are amalgamated in BBNP and preserve a section 32 m (105 ft) thick, comprised of middle Late Turonian–latest Turonian, Austin Chalk-equivalent strata. Austin Chalk-equivalent strata continue above 84.6 m (277.5 ft; Ernst Tinaja) and 85 m (279 ft; Hot Springs), with these horizons marking the base of the AHZ—a proxy for the base of the Coniacian (Cobban et al., 2008; Cooper and Cooper, 2014; 2014a; 2014b). An 8-9% faunal turnover suggested by calcareous nannofossil data at the Turonian/Coniacian Boundary is representative of a widespread Late Turonian regression in the KWIS (Corbett et al. 2014; Corbett and Watkins, 2013).

5.4 Sedimentation Rates in the Ernst Member

Correlation (COR)-derived sedimentation rate estimates for Ernst Tinaja are shown in Table 4. COR-derived sedimentation rate estimates range from 0.34–2.3 cm/kyr for LEF-equivalent strata, 0.75–2.24 cm/kyr for UEF-equivalent strata and 1.8–3.64 cm/kyr for Austin Chalk-equivalent strata at Ernst Tinaja. Weighted mean sedimentation rates for the Ernst Member at Ernst Tinaja include 1.45 cm/kyr for LEF-equivalent, 1.35 cm/kyr for UEF-equivalent and 2.72 cm/kyr for Austin Chalk-equivalent strata. Average Spectral Misfit (ASM)-derived sedimentation rates from Deluca (2016) range from 0.599-0.794 cm/kyr for LEF strata and 0.866-0.876 cm/kyr for UEF strata, and are used for comparison against the weighted average sedimentation rates for LEF- and UEF-equivalent strata of the Ernst Member in BBNP.

Differences in sedimentation rate for LEF- and UEF-equivalent strata between Ernst Tinaja and Lozier Canyon may be attributed to 1) accumulation of spatial and/or temporal error associated with picking surfaces for the chronostratigraphic framework and/or the astrochronology methods employed by Deluca (2016), 2) accumulation of temporal error associated with the presence of unidentified condensed intervals and/or disconformities in section (for both sections included in comparison), and 3) geologic controls on sedimentation (e.g., accommodation generated by differential compaction, subsidence, sediment supply and relative sea level fluctuations). Additional temporal error in the assignment of some temporal age ranges (e.g., 2σ uncertainty for CA-IDTIMS-dated bentonites) originates from uncertainty in the duration of the LEF/UEF boundary-equivalent hiatus in BBNP and from broad temporal ranges for biostratigraphic zones.

Sedimentation rate estimates for Mule Canyon are difficult to determine due to difficulties associated with isochron correlation caused by 1) lithologic variability, 2) geochemical variability and 3) poor biostratigraphic control between the platform and basin localities used in this study. Accumulated uncertainty from data anchoring surfaces projected into the Ojinaga Formation section at Mule Canyon precludes accurate determination of sedimentation rates at that locality.

6. CONCLUSIONS

The basal 52.7 m (173 ft) of Ernst Member strata of the Boquillas Formation at Ernst Tinaja, BBNP is equivalent to the Eagle Ford Group whereas strata above 52.7 m (173 ft) to the top of the Ernst Member (84.6 m; 277.5 ft) are interpreted as Austin Chalk-equivalent. Eagle Ford Group-equivalent sediments in BBNP contain abundant HCS and SCS and were deposited in relatively shallow water depositional environments within storm wave base (tens of meters of water depth). Both the Ernst Tinaja and Hot Springs localities in BBNP were deposited on the platform during the Early Cenomanian–Late Turonian.

Correlation of high-resolution CA-IDTIMS ages between stratigraphic sections on regional scales, when used concomitantly with a suite of chemostratigraphic data and biostratigraphic proxies, provides the basis for a robust, regional chronostratigraphic framework. In the future, this approach may be used provide the opportunity to evaluate the reliability of astrochronological methods in determining sedimentation rates for stratigraphic sections riddled with disconformities.

A flooding surface spanning up to 500-600 kyr in the strata laterally-equivalent to the Facies A of the Eagle Ford Group sub-divides Early and Middle Cenomanian sediments in west Texas. Early–Middle Cenomanian strata may represent LEF-equivalent deposition or may be temporally equivalent to the Maness Shale, Woodbine Group, Pepper Shale and/or False Buda of east and south Texas, respectively. The disconformity (K65 SB in BBNP) spanning the LEF- and UEF-equivalent units represents a ~0.8–1.3 myr

hiatus. In Ernst Tinaja, this disconformity is interpreted to occur within the burrowed foraminiferal wackestone/packstone at 27.4 m (90 ft).

The record of OAE2 and the C/T boundary is not preserved in BBNP, but is at least partially recorded at Lozier Canyon. Biostratigraphy suggests the Ojinaga Formation at Mule Canyon may be older than the onset of OAE2 and/or the C/T boundary. In BBNP however, an Early Turonian section of Facies C may record the recovery period immediately following OAE2. Immediately above this interval in BBNP is an expanded D facies (Lower Langtry), which may partially represent lowstand wedge deposits 4.6–5.8 m (16–19 ft) thick. A significant Late Turonian portion (32 m; 105 ft) of Austin Chalk-equivalent strata are recorded in BBNP, and is only known from the Maverick Basin. The Eagle Ford Group/Austin Chalk contact at ~52.7 m (173 ft) at BBNP may be disconformable due to a relatively abrupt change in sedimentation rate, spectral gamma ray and geochemical signatures across the boundary.

REFERENCES

Adkins, W.S., 1933, The Mesozoic systems: In The geology of Texas, University of Texas Bulletin 3232, p. 239-518.

Alego, T.J. and Rowe, H., 2012, Paleoceanographic applications of trace-metal concentration data: Chemical Geology, v. 324-325, p. 6-18.

Anderson, E.G., 1979, Basic Mesozoic study in Louisiana; The northern Coastal Plain region and the Gulf Basin Province: Louisiana Geological Survey Folio Series, v. 3, 58 pp.

Banner, J.L., 1995, Application of the trace element and isotope geochemistry of strontium to studies of carbonate diagenesis: Sedimentology, v. 42, p. 805-824.

Befus, K. S., Hanson, R. E., Lehman, T. M., and Griffin, W. R., 2008, Cretaceous basaltic phreatomagmatic volcanism in west Texas: maar complex at Pena Mountain, Big Bend National park: Journal of Volcanology and Geothermal Research, v. 173, no. 3, p. 245-264.

Bilodeau, W.L., 1986, The Mesozoic Mogollon Highlands, Arizona: An Early Cretaceous Rift Shoulder: Geology, v. 94, no. 5, p. 724-735.

Blackburn, T. J., Olsen, P. E., Bowring, S. A., McLean, N. M., Kent, D. V., Puffer, J., McHone, G., Rasbury, E.T. and Et-Touhami, M., 2013, Zircon U-Pb geochronology links the end-Triassic extinction with the Central Atlantic Magmatic Province: Science, v. 340, no. 6135, p. 941-945.

Bowring, S. A., Schoene, B., Crowley, J. L., Ramezani, J., and Condon, D. J., 2006, High-precision U-Pb zircon geochronology and the stratigraphic record: Progress and promise: Paleontological Society Papers, v. 12, no. 25, p. 23-43.

Cobban, W.A., Hook, S.C. and McKinney, K.C., 2008, Upper Cretaceous molluscan record along a transect from Virden, New Mexico, to Del Rio, Texas: New Mexico Geology, v. 30, no. 3, p. 75-92.

Cobban, W.A. and Hook, S.C., 1989. Mid-Cretaceous molluscan record from west-central New Mexico, In Southeastern Colorado Plateau, Anderson, O.J., Lucas, S.G., Love, D.W and Cather, S.M. (eds.) New Mexico Geological Society 40th Annual Fall Field Conference Guidebook, 345 pp.

Cobban, W.A. and Hook, S.C., 1980, The Upper Cretaceous (Turonian) Ammonite Family Coilopoceratidae Hyatt in the Western Interior of the United States: USGS Professional Paper 1192, 21 pl., p. 1-28.

Cooper, R.W., Stevens, J.B., Cooper, D.A. and Stevens, M.S., 2005, Proposed: Revise the Contact between Ernst and San Vicente Members, Boquillas Formation, Big Bend National Park, Trans-Pecos, Texas: *In* Geological Society of America Abstracts with Programs, v.37, no. 3, 6 pp.

Cooper, R.W., Cooper, D.A., Stevens, J.B. and Stevens, M.S., 2008, Geology of the Hot Springs Trail area, Ernst and San Vicente Members of the Boquillas Formation; *in* Cooper, D.A. (ed.), The southern extension of the Western Interior Seaway: Geology of Big Bend National Park and Trans-Pecos, Texas: 2008 Joint Annual Meeting of the Geological Society of America and the Houston Geological Society, pp. 24-33.

Cooper, D.A. and Cooper, R.W., 2014a, Mapping of the Late Cretaceous Allocrioceras hazzardi Zone, Boquillas Formation, Big Bend National Park, Texas: *In* Geological Society of America South-Central Section Meeting, March 17-18, 2014, Fayetteville, AR.

Cooper, D.A. and Cooper, R.W., 2014b, Chronocorrelation of the Turonian-Coniacian Stage Boundary in the Boquillas Formation, Big Bend Region, Texas – the Allocrioceras hazzardi Zone: Houston Geological Society General Luncheon Meeting, Houston, TX, March 26, 2014: Houston Geological Society Bulletin, p. 31-35.

Cooper, R.W. and Cooper, D.A., 2014, Field Guide to Late Cretaceous Geology of the Big Bend Region: Houston Geological Society, 94 pp.

Corbett, M.J., Watkins, D.K. and Pospichal, J.J., 2014, A quantitative analysis of calcareous nannofossil bioevents of the Late Cretaceous (Late Cenomanian-Coniacian) Western Interior Seaway and their reliability in established zonation schemes: Marine Micropaleontology, v. 109, p. 30-45.

Corbett, M.J. and Watkins, D.K., 2013, Calcareous nannofossil paleoecology of the mid-Cretaceous Western Interior Seaway and evidence of oligotrophic surface waters during OAE2: Palaeogeography, Palaeoclimatology, Palaeoecology, v. 392, p.510-523.

Daugherty, F.W. and Powell, J.D., 1963, Late Cretaceous Stratigraphy in Northern Coahuila, Mexico: Geological Notes: AAPG Bulletin, v.47, no. 12, p. 2059-2064.

Davis, D., 2017, Digital Outcrop Models of the Eagle Ford Group in Lozier Canyon, Terrell County, Texas: Texas A&M University, Unpublished Thesis, 128 pp.

DeJong, H.W. and Addy, S.K., 1992, Only relatively small production seen in basins of far West Texas, Trans-Pecos Texas (Part 1): Oil and Gas Journal, v. 90, no. 3, p. 59-65.

DeJong, H.W. and Addy, S.K., 1992, Broad view indicates hydrocarbon potential low in far West Texas, Trans-Pecos Texas (Part 2): Oil and Gas Journal, v. 90, no. 4, p. 97-102.

Deluca, M.J., 2016, Ash Bed Analysis of the Cretaceous Eagle Ford Shale Using ID-TIMS U-Pb Methods: Implications for Biostratigraphic Refinement and Correlations within the Western Interior Seaway: Texas A&M University, Unpublished Thesis, 68 pp.

Denne, R.A., Hinote, R.E., Breyer, J.A., Kosanke, T.H., Lees, J.A., Engelhardt-Moore, N., Spaw, J.M. and Tur, N., 2014, The Cenomanian-Turonian Eagle Ford Group of South Texas: Insights on timing and paleoceanographic conditions from geochemistry and micropaleontologic analyses: Palaeogeography, Palaoclimatology, Palaeoecology, v. 413, p. 2-28.

Denne, R.A, Breyer, J.A, Callender, A.D, Hinote, R.E., Kariminia, M., Kosanke, T.H., Kita, Z., Lees, J., Rowe, H., Spaw, J.M., and Tur, N., 2016, Biostratigraphic and Geochemical Constraints on the Stratigraphy and Depositional Environments of the Eagle Ford and Woodbine Groups of Texas. Chapter 1: Part 1 *In* Breyer, J.A. ed., The Eagle Ford Shale: A renaissance in U.S. oil production: AAPG Memoir, v. 110, p. 1-86.

Denne, R.A. and Breyer, J.A., 2016, Regional Depositional Episodes of the Cenomanian-Turonian Eagle Ford and Woodbine Groups of Texas. Chapter 1: Part 2 *In* Breyer, J.A., ed., The Eagle Ford Shale: A Renaissance in U.S. oil production: AAPG Memoir, v. 110, p. 87-133.

Desmares, D., Grosheny, D., Beaudoin, B., Gardin, S., and Gauthier-Lafaye, F., 2007, High resolution stratigraphic record constrained by volcanic ash beds at the Cenomanian–Turonian boundary in the Western Interior Basin, USA: Cretaceous Research, v. 28, no. 4, p. 561-582.

Dickinson, W.R., Klute, M.A. and Swift, P.N., 1986, The Bisbee Basin and its Bearing on Late Mesozoic Paleogeographic and Paleotectonic Relations between the Cordilleran and Caribbean Regions; Pacific Section SEPM, p. 51-62.

Donovan, A.D., Pope, M.C., Gardner, R.D. and Peavey, E.J., 2017, Field Guide to the Eagle Ford Group: West Texas: AAPG Field Seminar *In* AAPG ACE 2017, April 5-8.

Donovan, A.D., Staerker, T.S., Gardner, R., Pope, M.C., Pramudito, A. and Wehner, M., 2016, Findings from the Eagle Ford Outcrops of West Texas and Implications to the Subsurface of South Texas, *In* Breyer, J.A. ed., The Eagle Ford Shale: A renaissance in U.S. oil production: AAPG Memoir, v. 110, p. 301-356.

Donovan, A. D., Gardner, R.D., Pramudito, A., Staerker, T.S., Wehner, M., Corbett, M.J., Lundquist, J.J., Romero, A.M., Henry, L.C., Rotzien, J.R. and Boling, K.S., 2015, Chronostratigraphic Relationships of the Woodbine and Eagle Ford Groups Across Texas: Gulf Coast Association of Geologic Societies, v. 4, p. 37-41.

Donovan, A.D., Staerker, T.S., Pramudito, A., Li, Weiguo, Corbett, M.J., Lowery, C.M., Romero, A.M. and Gardner, R.D., 2012, The Eagle Ford Outcrops of West Texas: A Laboratory for Understanding Heterogeneities within Unconventional Mudstone Reservoirs: Gulf Coast Association of Geological Societies, v. 1, p. 162-185.

Donovan, A. D., and Staerker, T. S., 2010, Sequence stratigraphy of the Eagle Ford (Boquillas) Formation in the subsurface of South Texas and outcrops of West Texas: Gulf Coast Association of Geological Societies Transactions, v. 60, p. 864-899.

Duque-Botero, F., Maurrasse, J.M-R.F., Hickey-Vargas, R., Melinte, M.C., Jaffe, R., and Lopez-Oliva, J.G., 2008, Microspheroid Accumulations and Geochemical Characteristics of a Cenomanian-Turonian Anoxic Basin: The Record of the Indidura Formation, NE Mexico: SEPM Special Publication 93, p. 1-16.

Elder, W.P., 1988, Geometry of Upper Cretaceous bentonite beds: Implications about volcanic source areas and paleowind patterns, western interior, United States: Geology, v. 16, p. 835-838.

Eldrett, J.S., Minisini, D. and Bergman, S.C., 2014, Decoupling of the carbon cycle during Ocean Anoxic Event 2: Geology, v. 42, no. 7, p. 567-570.

Eldrett, J. S., Ma, C., Bergman, S. C., Lutz, B., Gregory, F. J., Dodsworth, P., Phipps, M., Hardas, P., Minisini, D., Ozkan, A., Ramezani, J., Bowring, S.A., Kamo, S.L., Ferguson, K., Macaulay, C. and Kelly, A. E., 2015, An astronomically calibrated stratigraphy of the Cenomanian, Turonian and earliest Coniacian from the Cretaceous Western Interior Seaway, USA: Implications for global chronostratigraphy: Cretaceous Research, v. 56, p. 316-344.

Elrick, M., Molina-Garza, R., Duncan, R. and Snow, L., 2009, C-Isotope stratigraphy and paleoenvironmental changes across OAE2 (mid-Cretaceous) from shallow-water platform carbonates of southern Mexico: Earth and Planetary Science Letters, v. 277, p. 295-306.

Ewing, T., 2013, Eagle Ford – Colorado Connection: Cenomanian to Coniacian in Southwestern North America: *In* AAPG Rocky Mountain Section Meeting, Salt Lake City, Utah, September 22-24.

Ferrill, D.A., Morris, A.P., Wigginton, S.S., Smart, K.J., McGinnis, R.N., and Lehrmann, D., 2016, Deciphering thrust fault nucleation and propagation and the importance of footwall synclines: Journal of Structural Geology, v. 85, p. 1-41.

Flores, A.L., 2013, Occurrence of a tylosaurine mosasaur (Mosasauridae; Russellosaurina) from the Turonian of Chihuahua State, Mexico: Boletín de la Sociedad Geológica Mexicana, v.65, no. 1, p. 1-9.

Frébourg, G., Ruppel, S.C., Loucks, R.G. and Lambert, J., 2016, Depositional controls on sediment body architecture in the Eagle Ford/Boquillas system: Insights from outcrops in west Texas, United States: AAPG Bulletin, v. 100, no. 4, p. 657-682.

Freeman, V.L., 1968, Geology of the Comstock-Indian Wells Area, Val Verde, Terrell and Brewster Counties, Texas: Geological Survey Professional Paper 594-K, K 1-26.

Frush, M.P. and Eicher, D.L., 1975, Cenomanian and Turonian Foraminifera and Palaeoenvironments in the Big Bend Region of Texas and Mexico: The Geological Association of Canada Special Papers, v. 13, p. 277-301.

Gale, A.S., Hardenbol, J., Hathaway, B., Kennedy, W.J., Young, J.R. and Phansalkar, V., 2002, Global correlation of Cenomanian (Upper Cretaceous) sequences: Evidence for Milankovitch control on sea level: Geology, v. 30, p. 291-294.

Gardner, R.D., Pope, M.C., Wehner, M.P. and Donovan, A.D., 2013, Comparative Stratigraphy of the Eagle Ford Group Strata in Lozier Canyon and Antonio Creek, Terrell County, Texas: Gulf Coast Association of Geological Societies, v. 2, p. 42-52.

Gilbert, G.K., 1895, Sedimentary Measurement of Cretaceous Time: The Journal of Geology, v. 3, no. 2, p. 121-127.

Goldhammer, R.K. and Johnson, C.A., 2001, Middle Jurassic-Upper Cretaceous Peleogeographic Evolution and Sequence-stratigraphic Framework of the

Northwest Gulf of Mexico Rim: *In* C. Bartolini, R.T. Buffler, and A. Cantú-Chapa, eds., The western Gulf of Mexico Basin: Tectonics, sedimentary basins, and petroleum systems: AAPG Memoir, v. 75, p. 45-81.

Gradstein, F.M., Ogg, J.G., Schmitz, M.D. and Ogg, G.M., 2012, The Geologic Time Scale 2012, Elsevier, 1176 pp.

Grosskopf, J.F., 2015, Chapter 2: Trace Fossils and Sediment Accumulation Rates from Cretaceous Western Interior Seaway Outcrops Evidence Variable Benthic Oxygen Conditions for the Duration of the OAE II Interval: Louisiana State University, Unpublished Dissertation, 56 pp.

Haenggi, W.T., 2002, Tectonic history of the Chihuahua trough, Mexico and adjacent USA, Part II: Mesozoic and Cenozoic: Boletín de la Sociedad Geológica Mexicana, v. 55, no. 1, p. 38-94.

Hennings, P.H., 1994, Structural transect of the southern Chihuahua Fold Belt between Ojinaga and Aldama, Chihuahua, Mexico: Tectonics, v. 13, no. 6, p. 1445-1460.

Haq, B.U., Hardenbol, J. and Vail, P.R., 1987, Chronology of fluctuating sea levels since the Triassic (250 million years ago to present): Science, v. 235, p. 1159-1167.

Haq, B.U., 2014, Cretaceous eustasy revisited: Global and Planetary Change, v. 114, p. 44-58.

Hays, J. D., Imbrie, J., and Shackleton, N. J., 1976, Variations in the Earth's orbit: pacemaker of the ice ages: Science, v. 192, no. 4270, p. 1121-1132.

Hentz, T.F., Ambrose, W.A. and Smith, D.C., 2014, Eaglebine play of the southwestern East Texas Basin: Stratigraphic and depositional framework of the Upper Cretaceous (Cenomanian-Turonian) Woodbine and Eagle Ford Groups: AAPG Bulletin, v. 98, no. 12, p. 2551-2580.

Hentz, T.F. and Ruppel, S.C., 2010, Regional Lithostratigraphy of the Eagle Ford Shale: Maverick Basin to East Texas Basin: Gulf Coast Association of Geological Societies Transactions, v. 60, p. 325-337.

Hildebrand, R.S., 2015, Dismemberment and northward migration of the Cordilleran orogeny: Baja-BC resolved: GSA Today, v. 25, no. 11, p. 4-11.

Hinnov, L. A., 2013, Cyclostratigraphy and its revolutionizing applications in the earth and planetary sciences: Geological Society of America Bulletin, v. 125, no. 11-12, p. 1703-1734.

Kauffman, E.G., 1977, Geological and Biological overview: Western Interior Cretaceous Basin: Mountain Geologist v. 14, no. 3-4, p. 75-99.

Kauffman, E.G. and Caldwell, W.G.E., 1994, The Western Interior Basin in space and time. In Caldwell, W.G.E., Kauffman, E.G. eds., Evolution of the Western Interior Basin: Geological Association of Canada Special Paper, v. 39, p. 1-30.

Kennedy, W.J., Cobban, W.A., Hancock, J.M. and Hook, S.C., 1989, Biostratigraphy of the Chispa Summit Formation at its type locality: a Cenomanian through Turonian reference section for Trans-Pecos Texas: Bulletin of the Geological Institutions of the University of Uppsala, N.S., v. 15, p. 39-119. Uppsala ISSN 0302-2749.

Kennedy, W.J., Walaszczyk, I. and Cobban W.A., 2000, Pueblo, Colorado, USA, candidate Global Boundary Stratotype Section and Point for the base of the Turonian State of the Cretaceous and for the base of the idle Turonian Substage, with a revision of the Inceramidae (Bivalvia): Acta geologica Polonica, v. 50, no. 3, p. 295-334.

King, R.E. and Adkins, W.S., 1946, Geology of a Part of the Lower Conchos Valley, Chihuahua, Mexico: Geological Society of America Bulletin, v. 57, p. 275-294.

Kuroda, J., Ogawa, N.O., Tanimizu, M., Coffin, M.F., Tokuyama, H., Kitazato, H., and Ohkouchi, N., 2007, Contemporaneous massive subaerial volcanism and Late Cretaceous Oceanic Anoxic Event 2: Earth and Planetary Science Letters, v. 256, p. 211-223.

Lock, B.E., Bases, F.S. and Glaser, R.A., 2007, The Cenomanian sequence stratigraphy of central to West Texas: Gulf Coast Association of Geological Societies Transactions, v. 57, p. 465-479.

Lowery, C. M., Corbett, M. J., Leckie, R. M., Watkins, D., Romero, A. M., and Pramudito, A. (2014). Foraminiferal and calcareous nannofossil paleoecology and paleoceanography of the Cenomanian–Turonian Eagle Ford Shale of southern Texas. Palaeogeography, Palaeoclimatology, Palaeoecology, 413, 49-65.

Martini, M., and Ortega-Gutiérrez, F., 2016, Tectono-stratigraphic evolution of eastern Mexico during the break-up of Pangea: A review: Earth-Science Review, (In Press), 18 pp.

Mattinson, J. M., 2013, Revolution and evolution: 100 years of U–Pb geochronology: Elements, v. 9, no. 1, p. 53-57.

Mattinson, J. M., 2011, Extending the Krogh legacy: development of the CA-TIMS method for zircon U-Pb geochronology This article is one of a series of papers published in this Special Issue on the theme of Geochronology in honour of Tom Krogh: Canadian Journal of Earth Sciences, v. 48, no. 2, p. 95-105.

Maxwell, R.A., Lonsdale, J.T., Hazzard, R.T. and Wilson, J.A., 1967, Geology of Big Bend National Park, Brewster County, Texas: University of Texas at Austin, Bureau of Economic Geology Publication 6711, 320 pp.

Meyers, S. R., 2012, Seeing red in cyclic stratigraphy: Spectral noise estimation for astrochronology: Paleoceanography, v. 27, no. 3, p. 1-12.

Meyers, S. R., and Sageman, B. B., 2007, Quantification of deep-time orbital forcing by average spectral misfit: American Journal of Science, v. 307, no. 5, p. 773-792.

Meyers, S. R., Sageman, B. B., and Hinnov, L. A., 2001, Integrated quantitative stratigraphy of the Cenomanian-Turonian Bridge Creek Limestone Member using evolutive harmonic analysis and stratigraphic modeling: Journal of Sedimentary Research, v. 71, no. 4, p. 628-644.

Meyers, S. R., Siewert, S. E., Singer, B. S., Sageman, B. B., Condon, D. J., Obradovich, J. D., Jicha, B.R. and Sawyer, D. A., 2012, Intercalibration of radioisotopic and astrochronologic time scales for the Cenomanian-Turonian boundary interval, Western Interior Basin, USA: Geology, v. 40, no. 1, p. 7-10.

Miller, R.W., 1990, The Stratigraphy and Depositional Environment of the Boquillas Formation of southwest Texas: Unpublished Thesis from University of Arlington, 156 pp.

Molenaar, C.M., 1983, Major Depositional Cycles and Regional Correlations of Upper Cretaceous Rocks, Southern Colorado Plateau and Adjacent Areas: *In* Mesozoic Paleogeography of the West-Central United States: Rocky Mountain Paleogeography Symposium 2: SEPM Rocky Mountain Section, p. 201-224.

Moustafa, A.R., 1988, Structural Geology of Sierra del Carmen, Trans-Pecos Texas. 1:48,000 scale geologic map: Geologic Quadrangle Map 54, Bureau of Economic Geology: The University of Texas at Austin.

Ogg, J.G., Agterberg, F.P. and Gradstein, F.M., 2004, A Geologic Time Scale 2004: *In* Geological Society of America Abstracts with Programs, v. 36, p.74.

Park, J. and Herbert, T.D., 1987, Hunting for Paleoclimatic Periodicities in a Geologic Time Series with an Uncertain Time Scale: Journal of Geophysical Research v. 92, no. B13, p. 14027-14040.

Pearce, T.J. and Jarvis, I., 1992, Applications of geochemical data to modelling sediment dispersal patterns in distal turbidites: Late Quarternary of the Madeira Abyssal Plain: Journal of Sedimentary Petrology, v. 62, p. 1112-1129.

Pearce, T.J., Besly, B.M., Wray, D.S. and Wright, D.K., 1999, Chemostratigraphy: a method to improve interwell correlation in barren sequences — a case study using onshore Duckmantian/Stephanian sequences (Wed Midlands, U.K.): Sedimentary Geology, v. 124, p. 197-220.

Pessagno, E.A., 1967, Upper Cretaceous planktonic foraminifera from the western Gulf coastal plain: Palaeontographica Americana, v. 5, p. 243-445.

Pessagno, E.A., 1969, Upper Cretaceous stratigraphy of the western Gulf Coast area of Mexico, Texas, and Arkansas: GSA Memoir v. 111, 139 pp.

Pierce, J.D., 2014, U-Pb geochronology of the Late Cretaceous Eagle Ford Shale, Texas; Defining chronostratigraphic boundaries and volcanic ash source: The University of Texas at Austin, Unpublished Thesis, 144 pp.

Powell, J.D., 1965, Late Cretaceous Platform-Basin Facies, Northern Mexico and Adjacent Texas: AAPG Bulletin, v. 49, no. 5, p. 511-525.

Orth, C.J., Attrep, Jr., M., Quintana, L.R., Elder, W.P., Kauffman, E.G., Diner, R. and Villamil, T., 1993, Elemental abundance anomalies in the late Cenomanian extinction interval: a search for the source(s): Earth and Planetary Science Letters, v. 117, p. 189-204.

Sageman, B. B., Meyers, S. R., and Arthur, M. A., 2006, Orbital time scale and new C-isotope record for Cenomanian-Turonian boundary stratotype: Geology, v. 34, no. 2, p. 125-128.

Sageman, B. and Lyons, T., 2004, Geochemistry of Fine-grained Sediments and Sedimentary Rocks: *In* MacKenszie, F. ed. Sediments, Diagenesis and Sedimentary Rocks: Treatise on Geochemistry, v. 7, p. 115-118.

Sageman, B.B., Rich, J., Arthur, M.A., Birthfield, G.E. and Dean, W.E., 1997, Evidence for Milankovitch Periodicities in Cenomanian-Turonian Lithologic and Geochemical Cycles, Western Interior, USA: Journal of Sedimentary Research, v. 67, no. 2, p. 286-302.

Sageman, B.B., Rich, J., Arthur, M.A., Dean, W.E., Savrda, C.E. and Bralower, T.J., 1998, Multiple Milankovitch Cycles in the Bridge Creek Limestone (Cenomanian-Turonian), Western Interior Basin. Stratigraphy and

Paleoenvironments of the Cretaceous Western Interior Seaway, USA: SEPM Concepts in Sedimentology and Paleontology, v. 6, p. 153-171.

Seibertz, E., 1998, Evolution of the mid-Cretaceous in northern Mexico under paleoceanographic aspects: Revista Mexicana de Ciencias Geológicas, v. 15, no. 1, p. 87-90.

Shurr, G.W., Ludvigson, G.A., and Hammond, R.H., 1994, Perspectives on the Eastern Margin of the Cretaceous Western Interior Basin: Geological Society of America, Boulder: Special Paper 287, 264 pp.

Sinton, C.W. and Duncan, R.A., 1997, Potential links between ocean plateau volcanism and global ocean anoxia at the Cenomanian-Turonian boundary: Economic Geology, v. 92, p. 836-842.

Slingerland, R., Kump, L.R., Arthur, M.A., Fawcett, P.J., Sageman, B.B., and Barron, E.J., 1996, Estuarine circulation in the Turonian Western Interior seaway of North America: GSA Bulletin, v. 108, no. 7, p. 941-952.

Sloss, L.L., 1963, Sequences in the Cratonic Interior of North America: Geological Society of America Bulletin, v. 74, p. 93-114.

Sohl, N.F., Martínez, E.R., Salmerón-Ureña, P. and Soto-Jaramillo, F., 1991, Upper Cretaceous: *In* Salvador, A., eds., The Gulf of Mexico Basin: The Geology of North America: Geological Society of America, p. 205-244.

Tian, Y., Ayers, W.B. and McCain, D., 2013, The Eagle Ford Shale Play, South Texas: Regional Variations in Fluid Types, Hydrocarbon Production and Reservoir Properties, IPTC 2013: International Petroleum Technology Conference.

Tiedemann, N.S., 2010, The Sequence Stratigraphy of the Comanchean-Gulfian Interval, Big Bend National Park, west Texas: Ball State University, Unpublished Thesis, 117 pp.

Tribovillard, N., Alego, T.J., Lyons, T. and Riboulleau, A., 2006, Trace metals as paleoredox and paleoproductivity proxies: An update: Chemical Geology, v. 232, p. 12-32.

Turgeon, S.C. and Creaser, R.A., 2008, Cretaceous oceanic anoxic event 2 triggered by a massive magmatic episode: Nature (London), v. 454, p. 323-326.

Turner, B.W., Tréanton, J.A. and Slatt, R.M., 2015, The Use of Chemostratigraphy to Refine Ambiguous Sequence Stratigraphic Correlations in Marine Shales: An Example from the Woodford Shale, Oklahoma: *In* AAPG Southwest Section

Annual Convention, Wichita Falls, Texas, April 11-14: Search and Discovery Article #51181.

Turner, K. J., Berry, M. E., Page, W. R., Lehman, T. M., Bohannon, R. G., Scott, R. B., Miggins, D.P., Budahn, J.R., Cooper, R.W., Drenth, B.J., Anderson, E.D. and Williams, V.S., 2011, Geologic map of Big Bend National Park, Texas: US Department of the Interior, US Geological Survey, p. 1-84.

Udden, J.A., 1907, A Sketch of the Geology of the Chisos Country, Brewster County, Texas: Bulletin of the University of Texas, v. 1, no. 93, 101 pp.

White, T., Furlong, K. and Arthur, M., 2002, Forebulge migration in the Cretaceous Western Interior basin of the central United States: Basin Research, v. 14, p. 43-54.

Wehner, M., Tice, M. M., Pope, M. C., Gardner, R., Donovan, A. D., and Staerker, T. S., 2015, Anoxic, Storm Dominated Inner Carbonate Ramp Deposition of Lower Eagle Ford Formation, West Texas: *In* Unconventional Resources Technology Conference: Society of Petroleum Engineers, p. 1-19.

Wilson, J.L., 1990, Basement structural controls on Mesozoic carbonate facies in northeastern Mexico–a review: *In* Carbonate Platforms: Facies, Sequences and Evolution: IAS Special Publications, v. 9, p. 235-255.

Winker, C.D. and Buffler, R.T., 1988, Paleogeographic Evolution of Early Deep-Water Gulf of Mexico and Margins, Jurassic to Middle Cretaceous (Comanchean): AAPG Bulletin, v. 72, no. 3, p. 318-346.

Wu, H., Zhang, S., Hinnov, L. A., Jiang, G., Feng, Q., Li, H., and Yang, T., 2013, Time-calibrated Milankovitch cycles for the late Permian: Nature communications, v. 4, p. 1-8.

Young, K., 1986b, Cretaceous, Marine Inundations of the San Marcos Platform, Texas: Cretaceous Research, v. 7, p. 117-140.

APPENDIX A

A.1 *Figures and Tables*

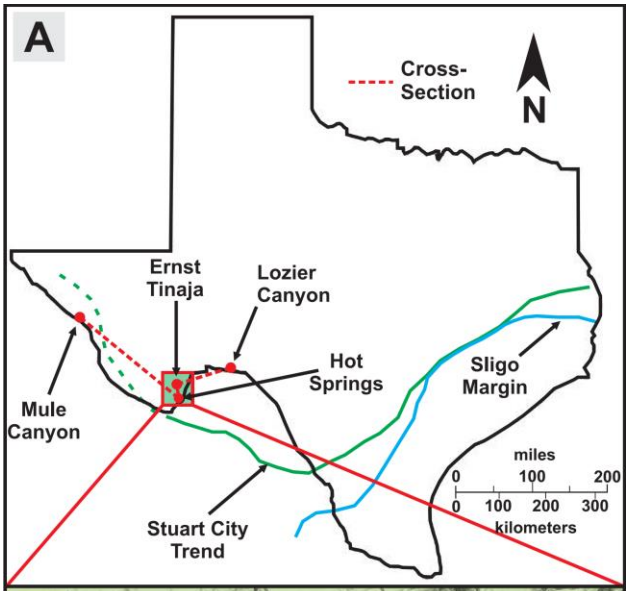

Figure 1. General map of Texas with all four localities utlized for this study **(A)**, zoomed image of study areas in Big Bend National Park used for sample collection and field data acquisition **(B)**.

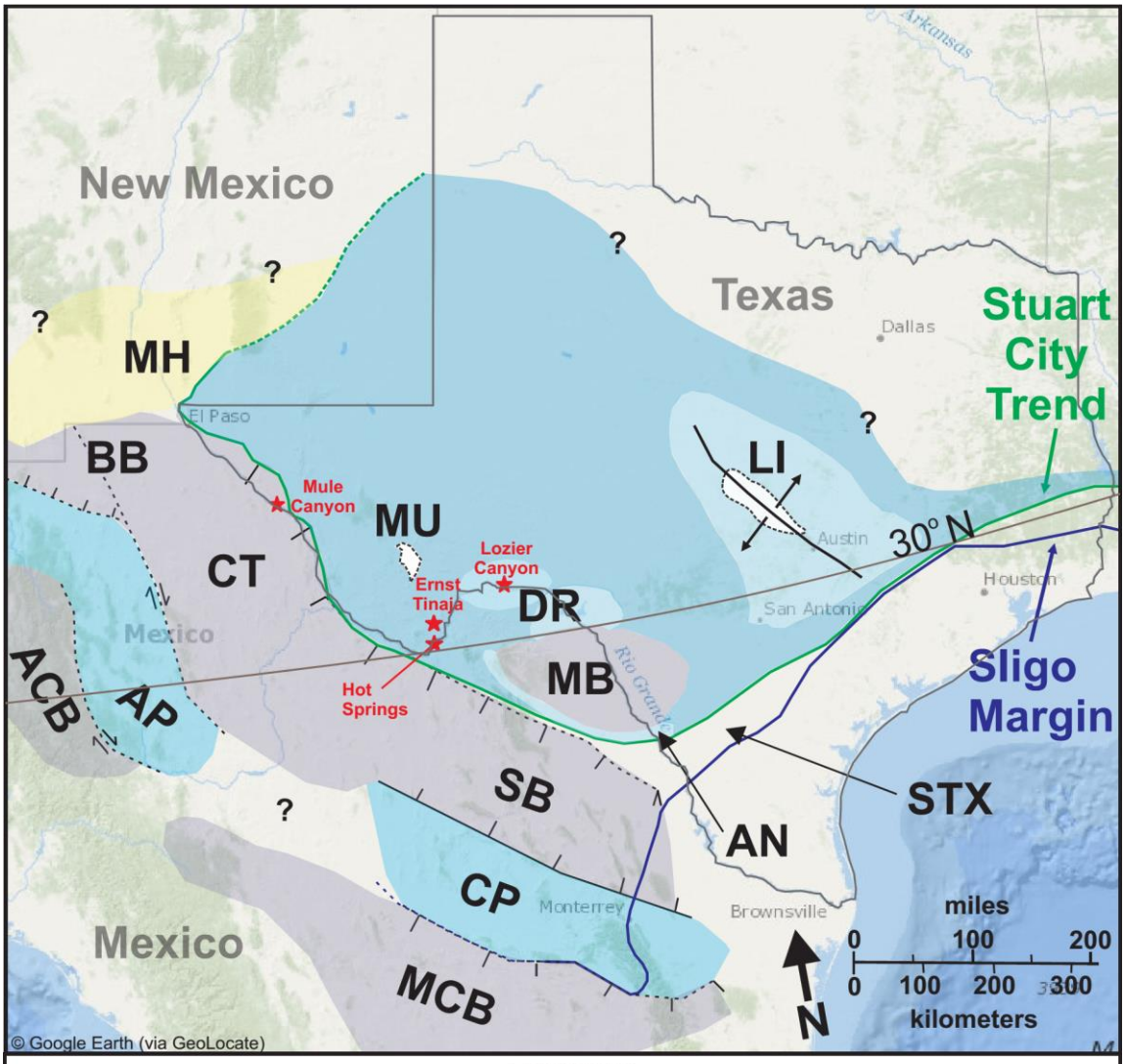

Figure 2. Paleogeographic reconstruction of the southern Cretaceous Western Interior Seaway (KWIS) during the Lower-Middle Cenomanian. Data from Bilodeau (1986), Corbett and Watkins (2013), DeJong and Addy (1992), Dickinson et al., (1986), Donovan et al., (2016), Donovan and Staerker (2010), Gardner et al. (2013), Hennings (1994), Martini and Ortega-Gutiérrez (2016) and Wilson (1990). Highlands in the northeast of Texas (e.g., Woodbine Deltas) are not included in this reconstruction. Reef margins are dashed where uncertain. 30°N latitude from Sageman et al., (1997).

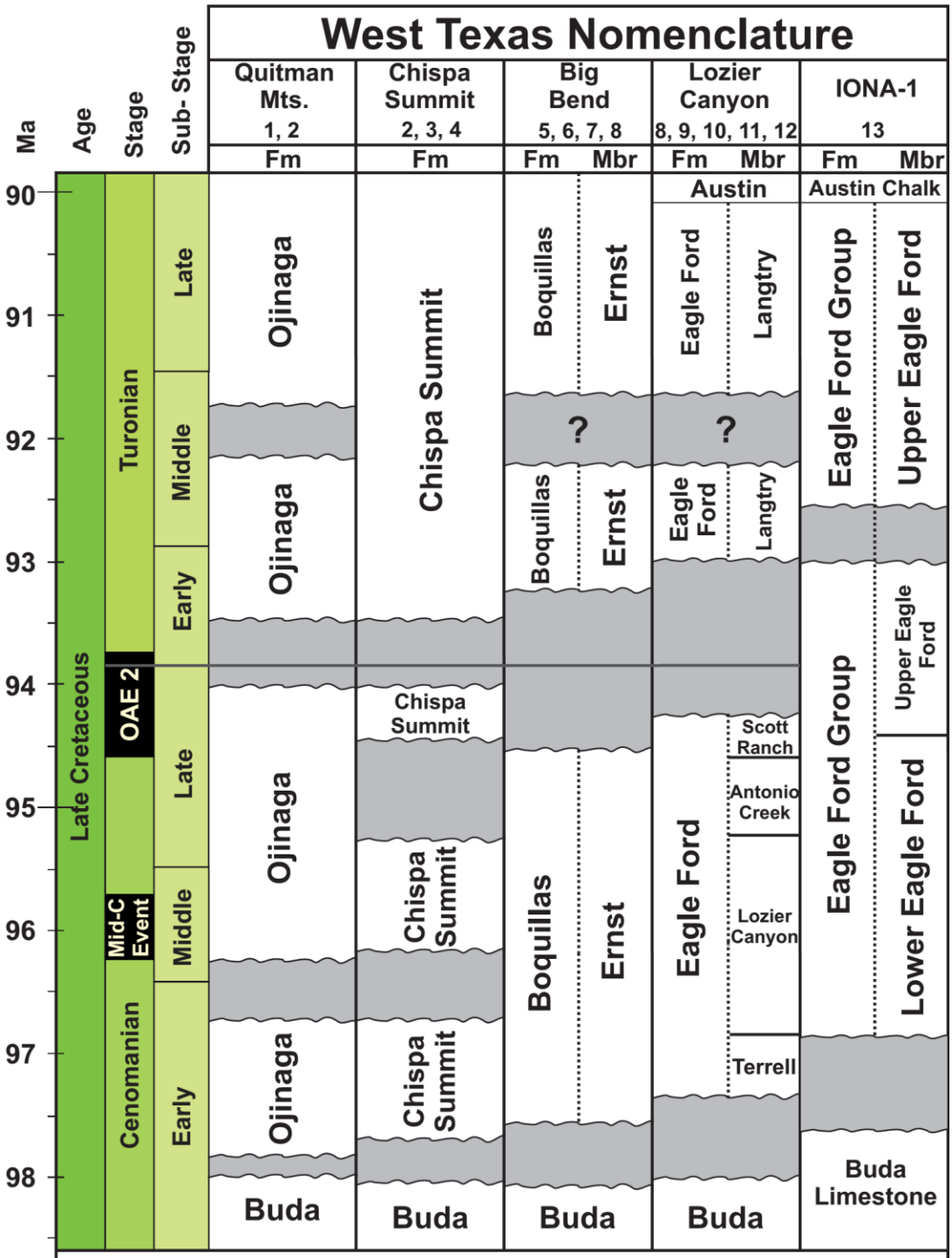

Figure 3. Eagle Ford-equivalent nomenclature in west Texas, modified from Denne et al., (2016). Data are derived from: **1.** Moore, 2016; **2.** Denne et al., 2016; **3.** Kennedy et al., 1989; **4.** King and Adkins, 1946; **5.** Maxwell et al., 1967; **6.** Cooper and Cooper, 2014; **7.** Wehner et al., 2015; **8.** Cobban et al., 2008; **9.** Donovan et al., 2012; **10.** Donovan and Staerker, 2010; **11.** Corbett et al., 2014; **12.** Deluca, 2016;**13.** Eldrett et al., 2015.

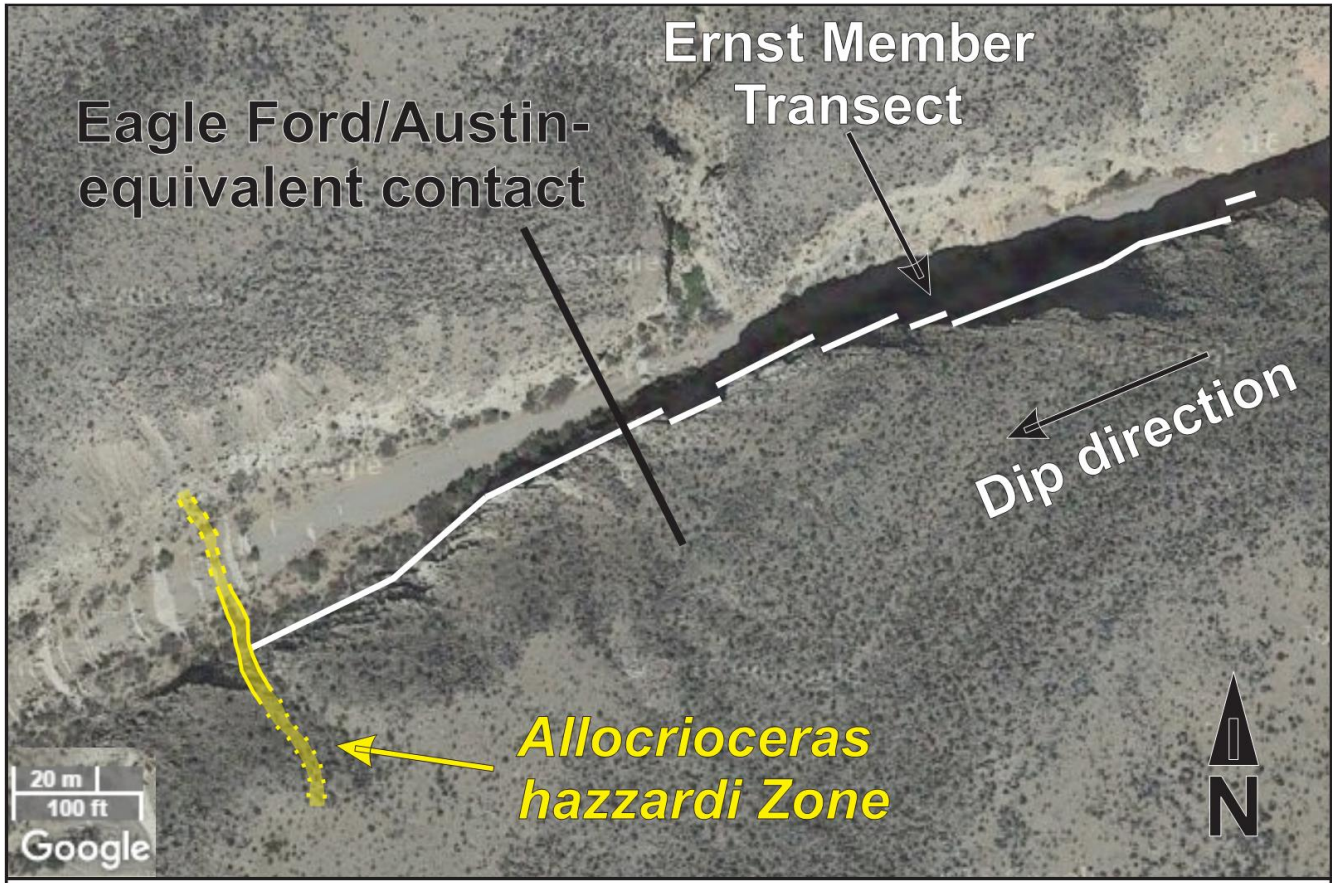

Figure 4. Aerial photo of the Ernst Tinaja locality. The white line trending WSW-ENE is the transect measured for this study. The black line dividing between the Eagle Ford- and Austin Chalk-equivalent strata of the Ernst Member is ~52.7 m (173 ft) above the base of the Ernst Member. The base of the *Allocrioceras hazzardi* Zone marks the top of the Ernst Member and base of the Coniacian. Strata dip ~13-21° towards the W-WSW.

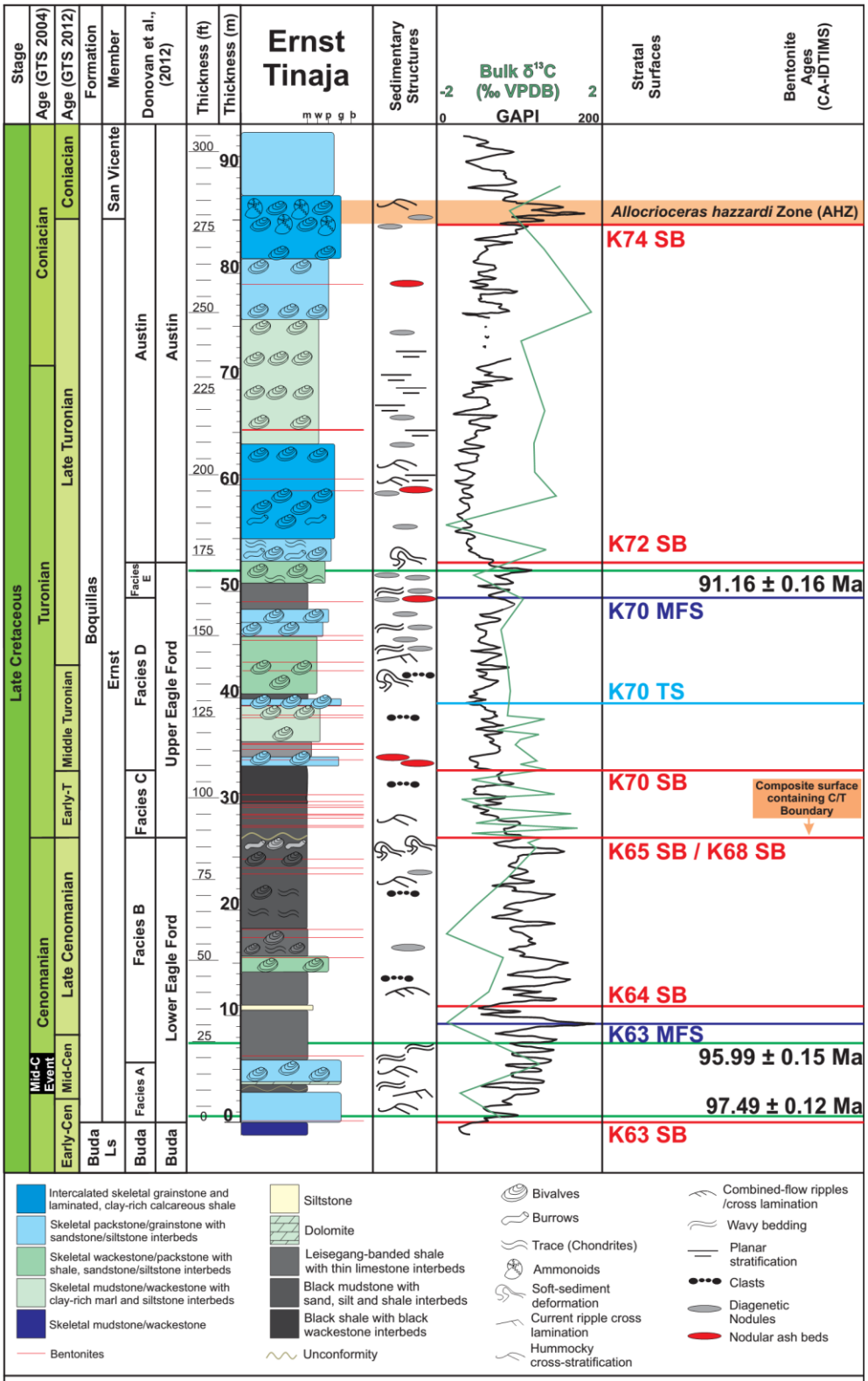

Figure 5. Stratigraphic column for the primary study locality, Ernst Tinaja, Big Bend National Park. Eagle Ford-equivalent strata span 0 - 52.7 m (0-173 ft), whereas Austin-equivalent strata span 52.7-93.3 m (173-306 ft; the top limit of lithostratigraphic analysis). The top of the Ernst Member is marked by the base of the *Allocrioceras hazzardi* zone at 84.6 m (277.5 ft; Cooper and Cooper, 2014).

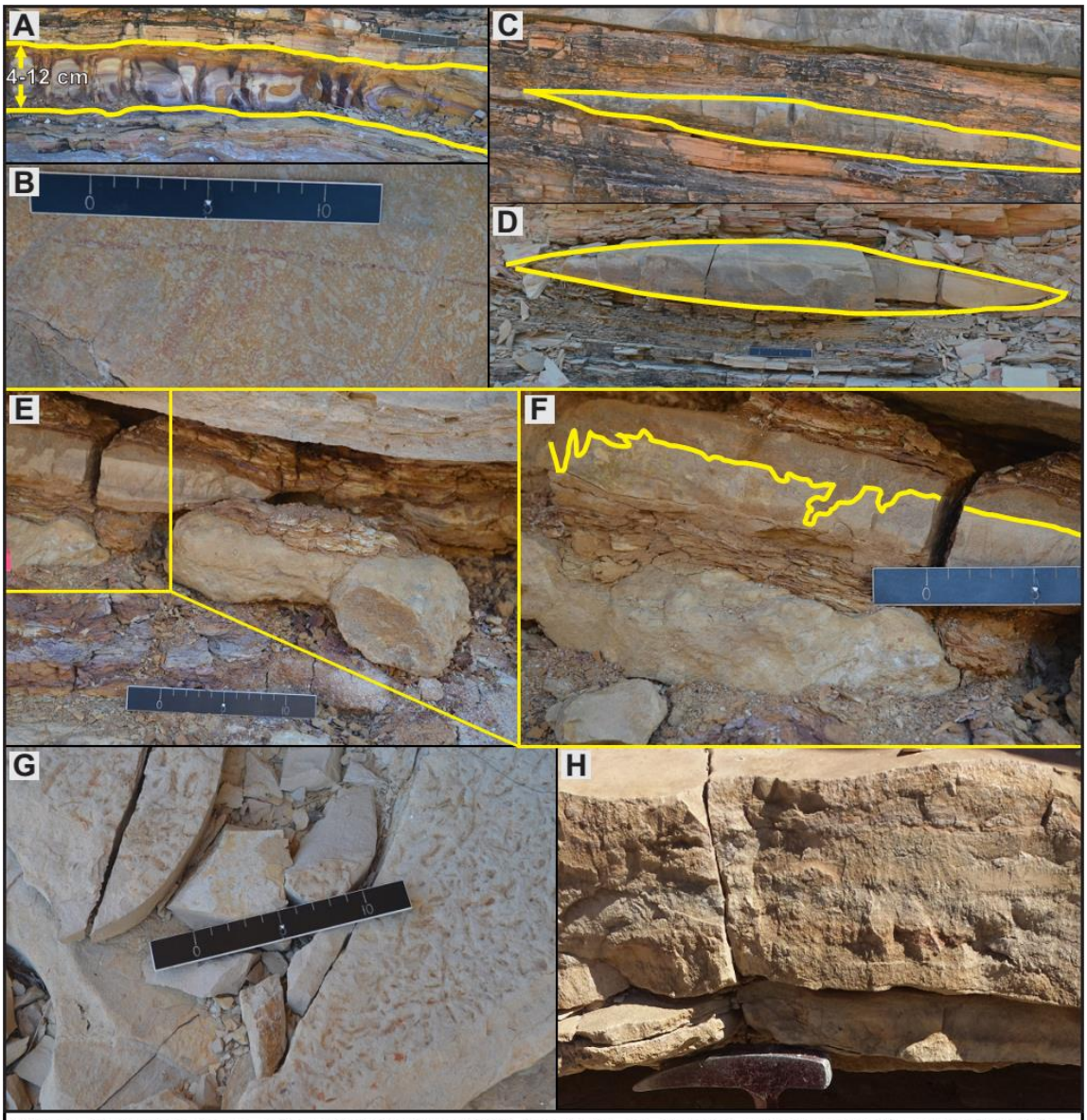

Figure 6. Near the base of the Ernst Member (**A**; 2.4 m (8 ft)), an unusual carbonate bed is cemented with Fe-oxide gangue (**B**) and Leisegang-banded with various colors, and has significant lateral thickness variations in Big Bend. Hummocky Cross Stratification (**C**; 8.5 m (28 ft)) and composite Hummocky/Swaley Cross Stratification (**D**; 12.2 m (40 ft)) is common the Eagle Ford-equivalent strata of the Ernst Member (basal 53.3 m (175 ft)). These symmetrical, lenticular beds have an average length of ~1-2 m (3-6 ft) and are an indicator of relatively shallow water deposition (near storm wave base). A cemented, burrowed, nodular foraminiferal grainstone bed (**E**; 27.4 m (90 ft)) varying ~0-12 cm in thickness was deposited between two bentonites (which fill the burrows with indurated material). In that same bed (**F**), burrows range 0-1 cm in diameter and are ~1-5 cm thick. Geochemical and biostratigraphic data suggest the bed marks the boundary between the Lower Eagle Ford (LEF) and Upper Eagle Ford (UEF). Ernst Tinaja is the only known locality to house a well-developed LEF/UEF disconformity in outcrop. *Chondrites* (**G**; 47.8 m (157 ft)) occur throughout the Ernst Member, but are ubiquitous in the strata laterally-equivalent to the Eagle Ford. These traces are primarily on the tops of limestone beds which have laterally-consistent thicknesses, and occasionally underlie bentonites. Wavy, indurated beds (**H**; ~52.5 m (173 ft)) are only present in a few places in section, including near the Eagle Ford Group/Austin Chalk-equivalent contact at ~52.7 m (173 ft) at Big Bend.

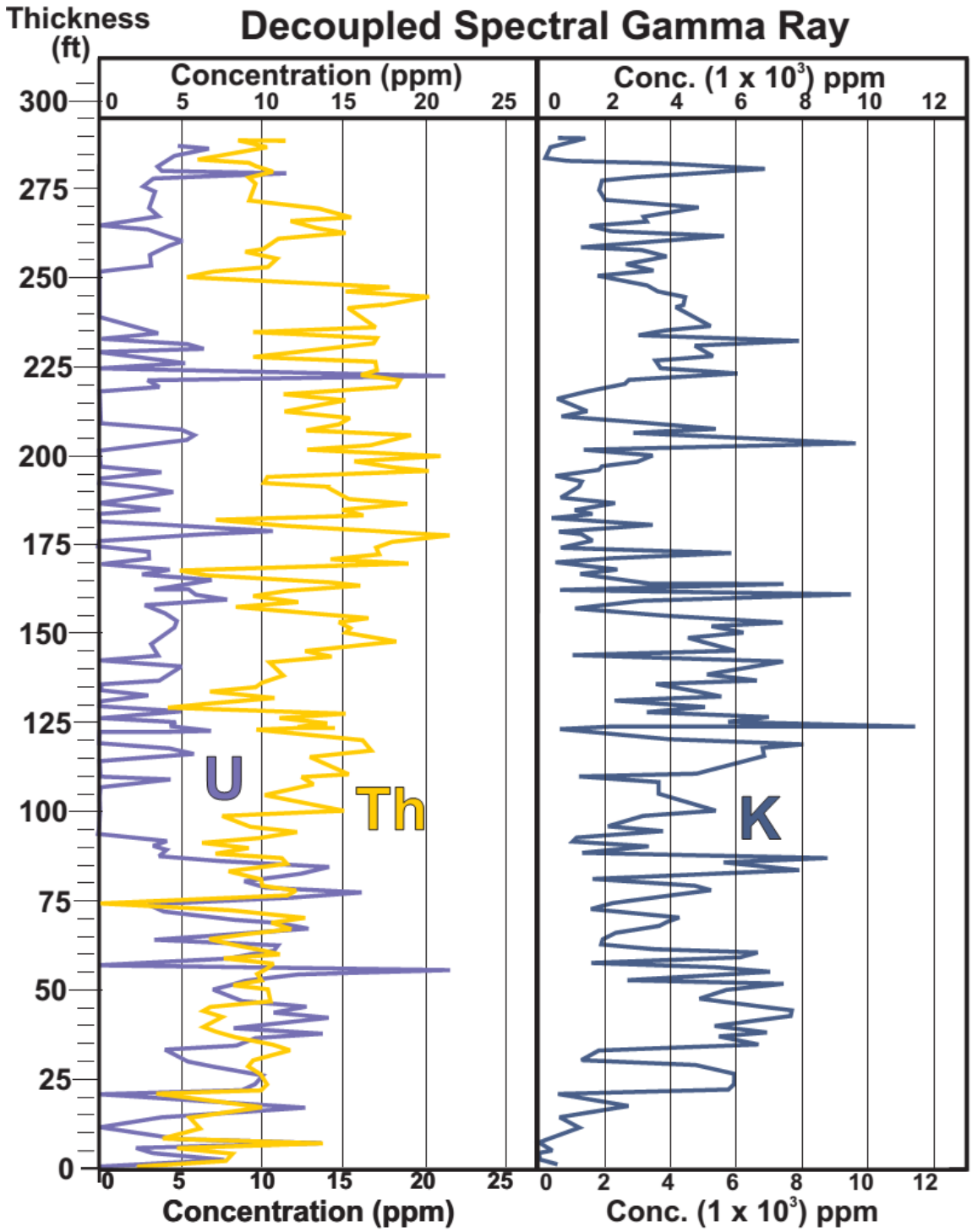

Figure 7. X-Ray Fluorescence plots of decoupled spectral gamma ray data for The Ernst Member type section at Ernst Tinaja, Big Bend National Park. Th spikes correspond to bentonites, U to reducing conditions in sediments, and K to siliciclastic influence on deposition.

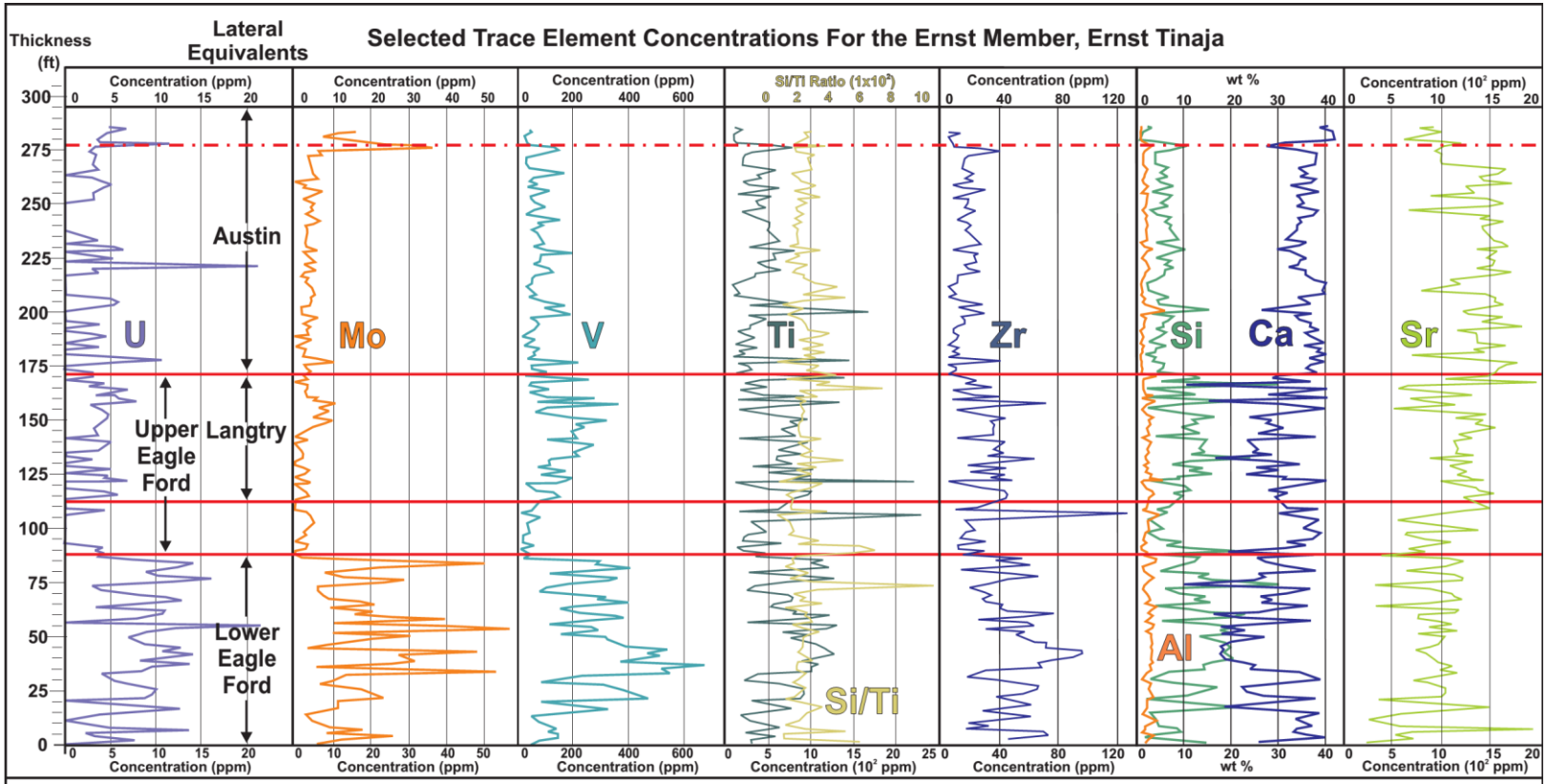

Figure 8. Selected trace element concentrations acquired with hand-held XRF. U, Mo and V provide information on redox conditions in a basin (Alego and Rowe, 2012; c.f. Tribovillard et al., 2006) and TOC content (e.g., if all high values, reducing conditions and high TOC are present). Ti and Zr are reliable proxies for siliciclastic sediment input (c.f. Sageman and Lyons, 2004; Tribovillard et al., 2006). The ratio between Si/Ti is a proxy for quartz content (c.f. Pearce and Jarvis, 1992; Pearce et al., 1999; Tribovillard et al., 2006). Ca and Sr are reliable carbonate proxies (c.f. Banner, 1995) and K and Al yield general information on clay content (c.f. Sageman and Lyons, 2004; Tribovillard et al., 2006). Additional information consulted for the generation of this figure can be found in Turner et al., (2015). The dash-dotted red line at 84.6 m (277.5 ft) is the boundary between the lower Ernst Member and upper San Vicente Member of the Boquillas Formation.

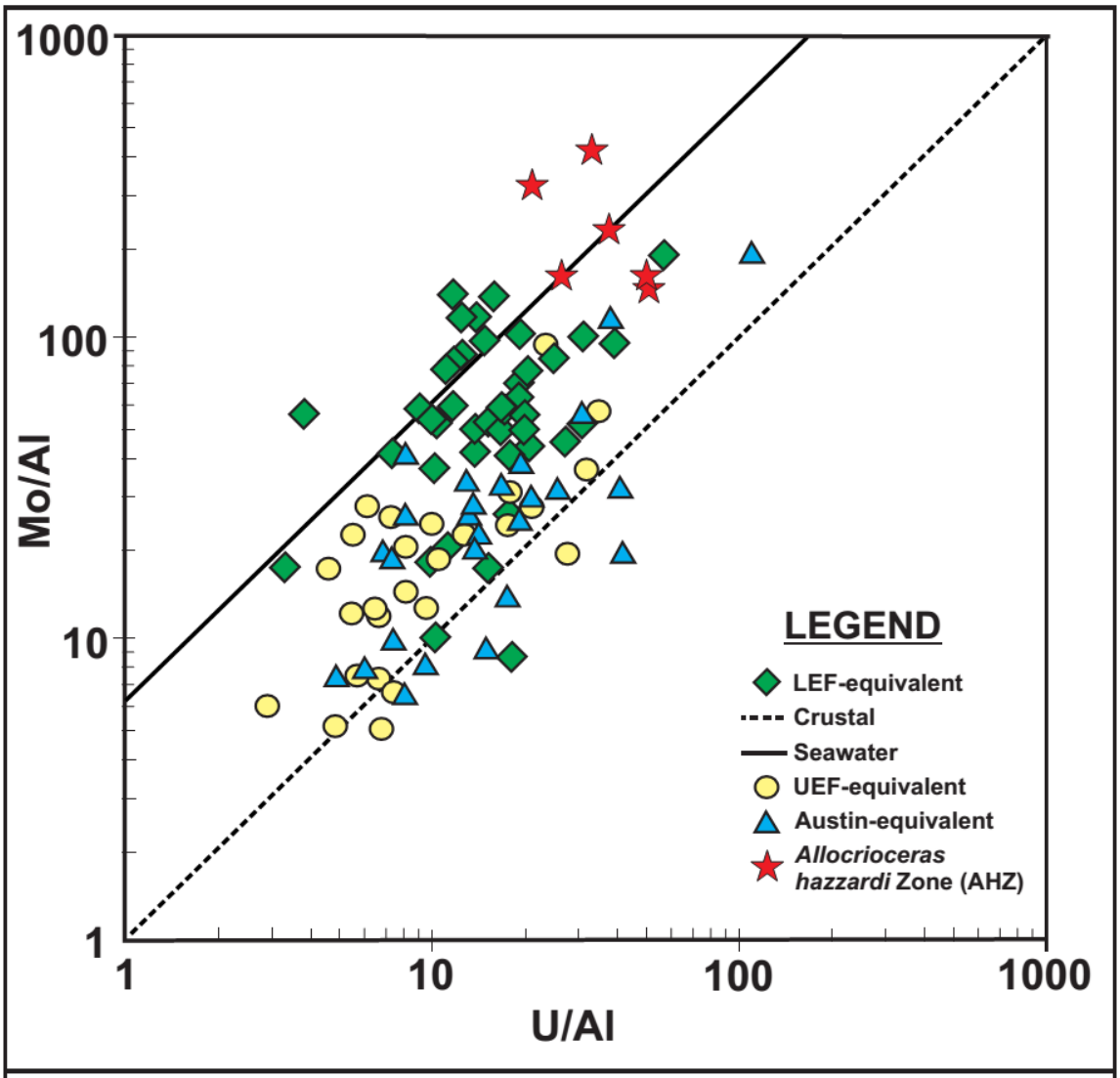

Figure 9. Logarithmic plot of Mo:U covariance for the Ernst Member type section at Ernst Tinaja, normalized with respect to Al. Individual values near the seawater curve suggest euxinia or anoxia persisted in the water column, whereas values closer to the crustal curve indicate local redox conditions were controlled more by crustal (terrigenous) input and anoxia more concentrated in sediments. All data points are within the Ernst Member except for AHZ data points, which are in the overlying San Vicente Member of the Boquillas Formation. Plot modeled after Eldrett et al., (2014).

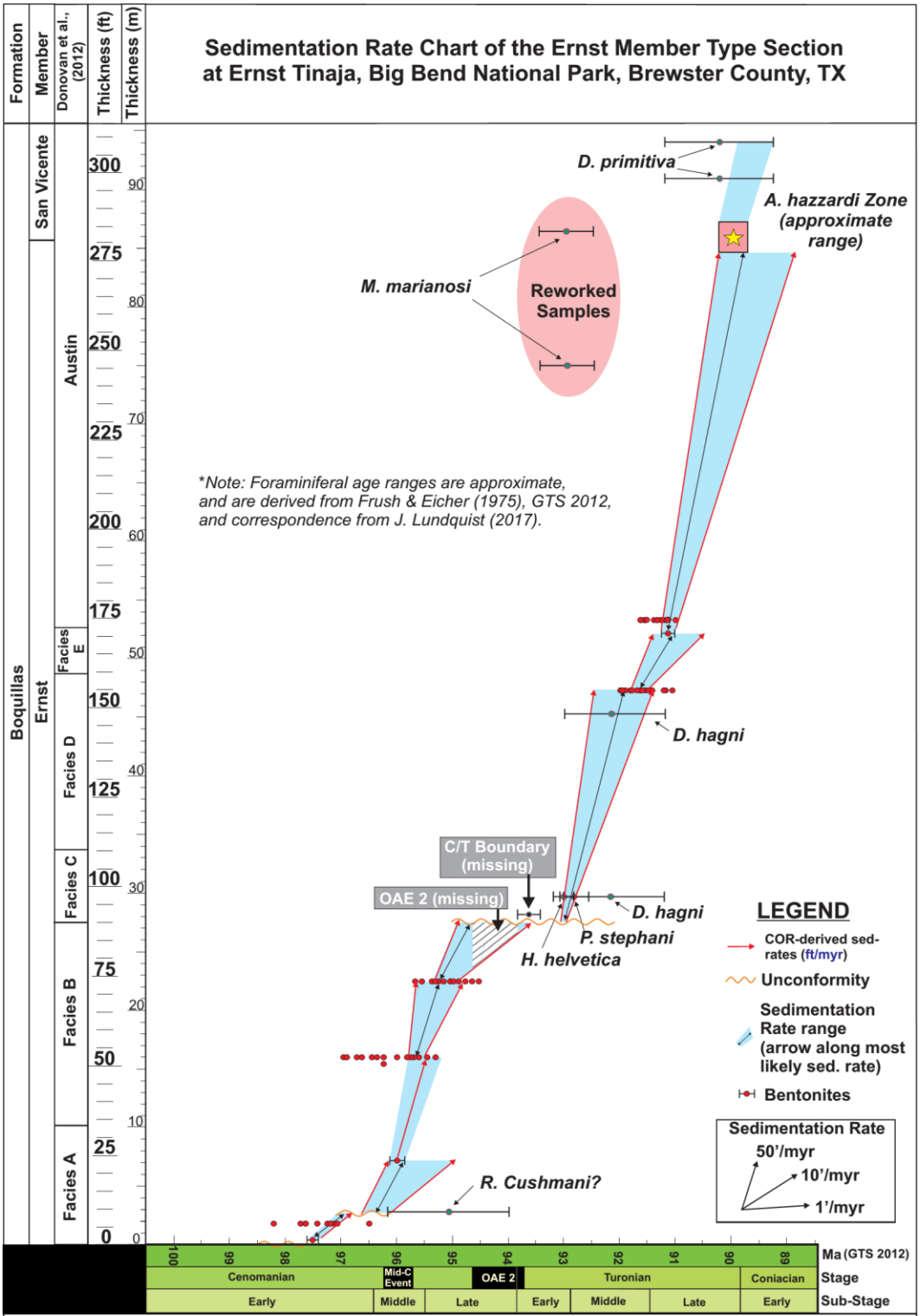

Figure 10. Sedimentation rates through time for the Ernst Member at Ernst Tinaja. All data in the figure adheres to the GTS 2012 (Gradstein et al., 2012). Individual zircon dates are indicated by small, red circles and were analyzed by Deluca (2016). Zircons correlated from Deluca (2016) into the Ernst Tinaja locality are based on bio- and chemostratigraphic data collected at Ernst Tinaja. Foraminifera samples processed for this study are included, as well as correlation (COR)-derived sedimentation rates (using isochrons and, in a single case, the geologic range of the *H. helvetica* Zone). Most likely sedimentation rates were calculated by honoring individual zircon ages, foraminifera and averaged, COR-derived sedimentation rates (Table 3) to constrain the base of each blue polygon (between each interval distinguished for the analysis).

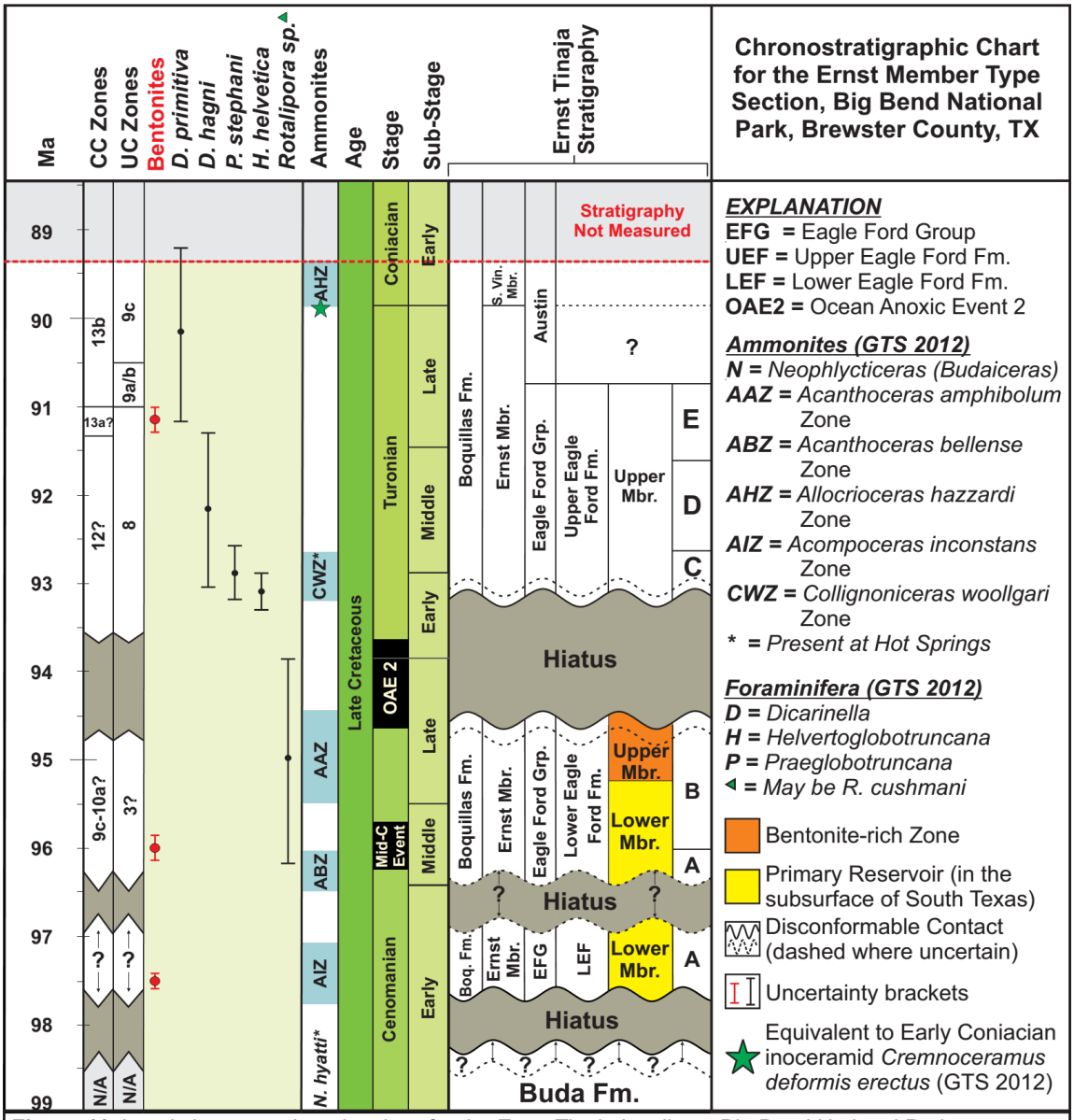

Figure 11. Local chronostratigraphy chart for the Ernst Tinaja locality at Big Bend National Park, Brewster County, Texas. All data for this figure is calibrated to the GTS 2012 (Gradstein et al., 2012). The Turonian/Coniacian boundary is defined as the base of the *Allocrioceras hazzardi* Zone, which is equivalent to the *Cremnoceramus deformis erectus* Zone from the Austin Chalk in North Texas. Facies A-E (right-most column) are interpreted lithostratigraphic equivalents to Lozier Canyon (Donovan et al., 2012). Uncertainty in duration of hiatuses is indicated by dashed lines. The lower boundary of the Buda/Ernst hiatus can be temporally constrained by the presence of *Neophylicticeras (Budaiceras) hyatti* ~1.3 m (5 ft) below the Buda/Ernst contact at Hot Springs 5.22 mi (8.24 km) SSW of Ernst Tinaja.

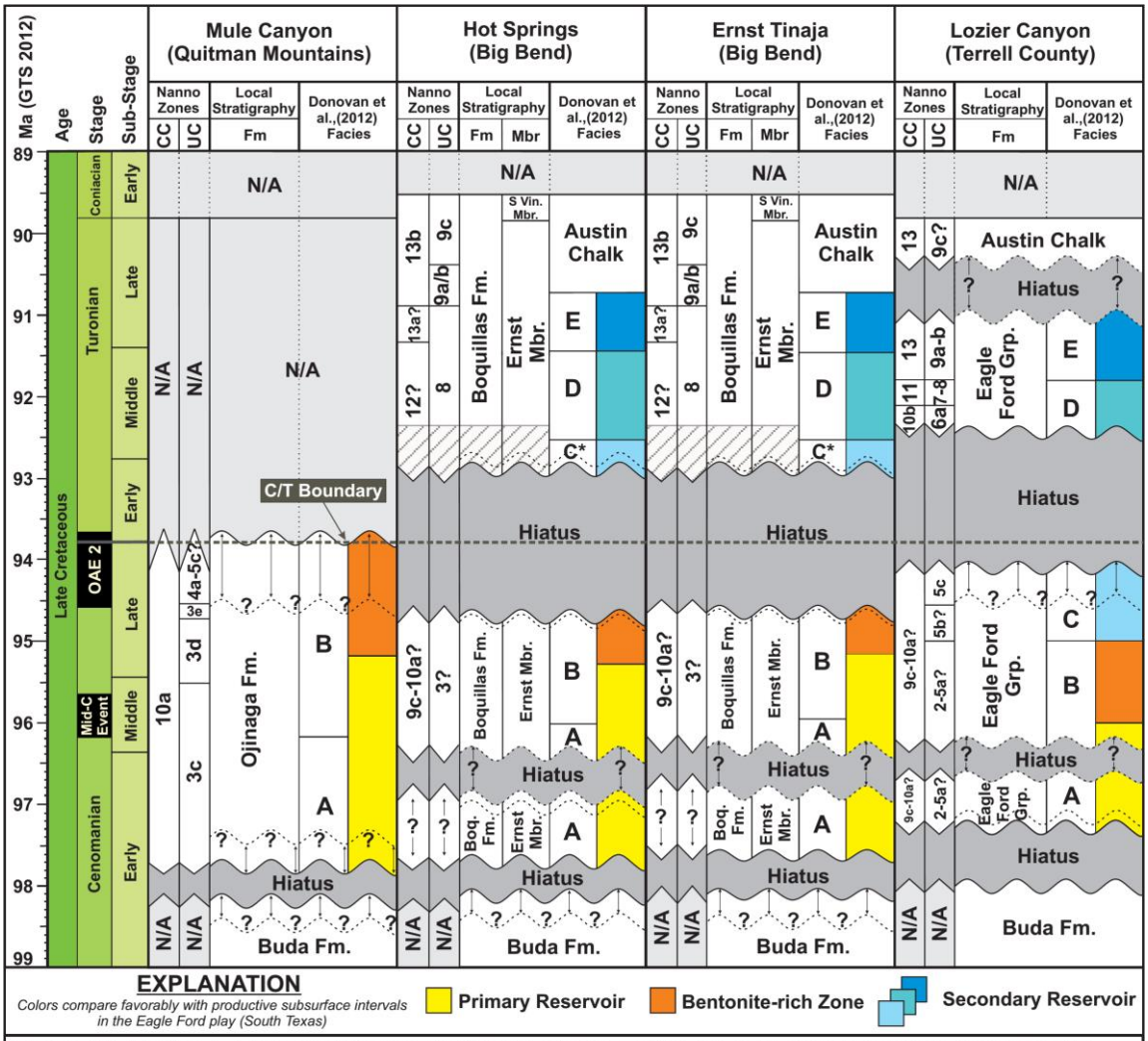

Figure 12. Regional chronostratigraphy chart for west Texas outcrops, using biostratigraphy (nannofossils, foraminifera and ammonites) and CA-IDTIMS-dated bentonite ages, supplemented by data from Deluca (2016), Gardner et al., (2013), Moore (2016), Corbett and Watkins (2014), Donovan et al., (2012) and Cooper and Cooper (2014). The basal 2.6 meters (~8 ft) of the Ernst Member at BBNP co-occurs with no known, formalized foraminifera zone and is beyond the lower sampling boundary for calcareous nannofossils (4.8 m; 16 ft) for this study. Hiatuses in this diagram, including the hiatus in the primary reservoir in the subsurface of south Texas is supported by foraminiferal and nannofossil biostratigraphy and CA-IDTIMS-dated bentonite ages. Extension of the primary reservoir hiatus into Lozier Canyon is supported by nannofossil, foraminiferal and ammonite biostratigraphy, as well as a CA-IDTIMS-dated bentonite age (97.14 ± 0.36 Ma) and similar chemostratigraphic signature (Wehner et al., 2015) in the basal 0.3 m (1 ft) at Lozier Canyon. The duration of the hiatus spanning 0.8-1.3 myr in Big Bend is supported by foraminiferal, ammonite and nannofossil biostratigraphy and the absence of the OAE2 positive CIE. Facies C* is a section of Facies C which represents Early Turonian deposition immediately following the occurrence of OAE2, and is coeval with a hiatus in Lozier Canyon. The hiatus at the Eagle Ford- and Austin Chalk-equivalent boundary at Big Bend and Lozier Canyon is expected to be of smaller duration than originally reported.Question marks denote uncertainty in hiatus duration.

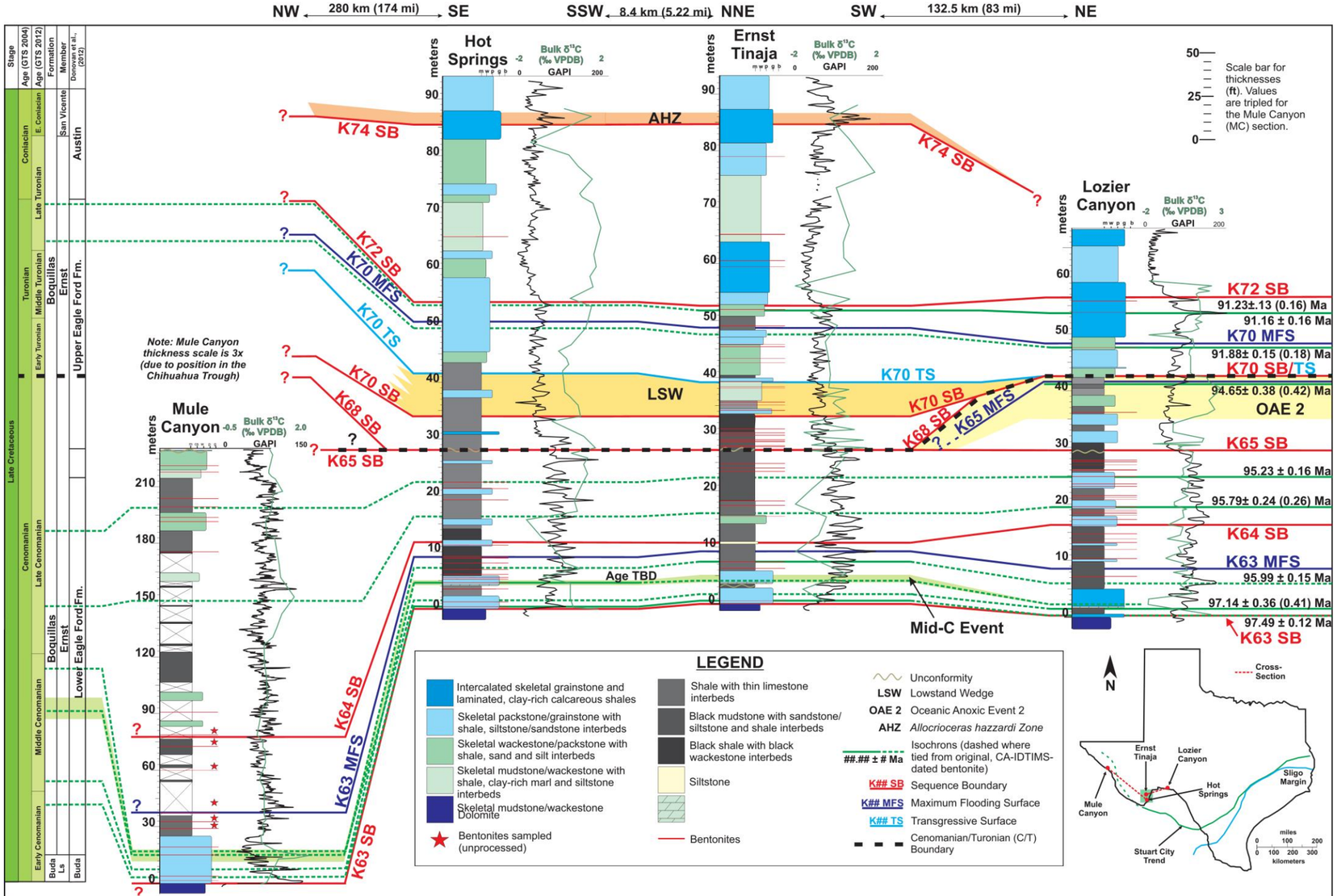

Figure 13. A chronostratigraphic framework for Cenomanian-Turonian strata in west Texas. Lithologies in stratigraphic columns are lumped, according to dominant lithology for any given interval of strata. Spectral gamma ray (SGR) data and bulk $\delta^{13}C$ data are presented with each section. Geochemical proxies (e.g., Si, Ca, Sr, K, Al, Zr, Ti, U, V, Mo) were utilized to chemostratigraphically constrain stratal surfaces. Nannofossil, foraminiferal and ammonite biostratigraphy were integrated with CA-IDTIMS bentonite ages (isochrons) to temporally constrain stratal surfaces and relative timing of isotopic events (e.g., OAE2 and Mid-Cenomianian Event). The interval between the K63 and K64 SBs is mostly laterally correlative with the hydrocarbon pay zone (primary reservoir) for the Eagle Ford shale play of south and central Texas. The stratigraphic interval between the K64 and K65 SBs is laterally correlative with the bentonite-rich zone, the base of which bounds the Eagle Ford shale play above. Stratal surfaces are tied only to lithostratigraphic facies (A-E), and are not tied to specific points in time with isochrons. Isochrons are correlated into a generalized GTS 2012 (Gradstein et al., 2012) timescale and are assigned relative positions in GTS sub stages. Early Cenomanian Eagle Ford-equivalent sediments are present in all four west Texas outcrop sections presented. The Mid-C Event occurs in Mule Canyon and Big Bend, but is thin at Lozier Canyon. The OAE2 is absent in both Big Bend localities studied, but is partially preserved at Lozier Canyon. An Early Turonian section of Donovan et al.'s, (2012) C-facies (equivalent to sub-facies C4/C5) is present in Big Bend, and is coincident with highstand and falling stage deposits (see Sageman et al.'s, (2006) carbon isotope curve for $\delta^{13}C$ comparison). Eagle Ford-equivalent deposition is defined here as occurring between the late Early Cenomanian and middle Late Turonian and is bounded below by the Early Cenomanian Buda Limestone and above by the Late Turonian-Santonian Austin Chalk (and lateral equivalents). The base of the *Allocrioceras hazzardi* Zone is coincident with the occurrence of an earliest Coniacian inoceramid *Cremnoceramus deformis erectus,* and is the Coniacian ammonite proxy for the southern KWIS; this boundary does not define the Eagle Ford/Austin Chalk-equivalent contact in Big Bend.

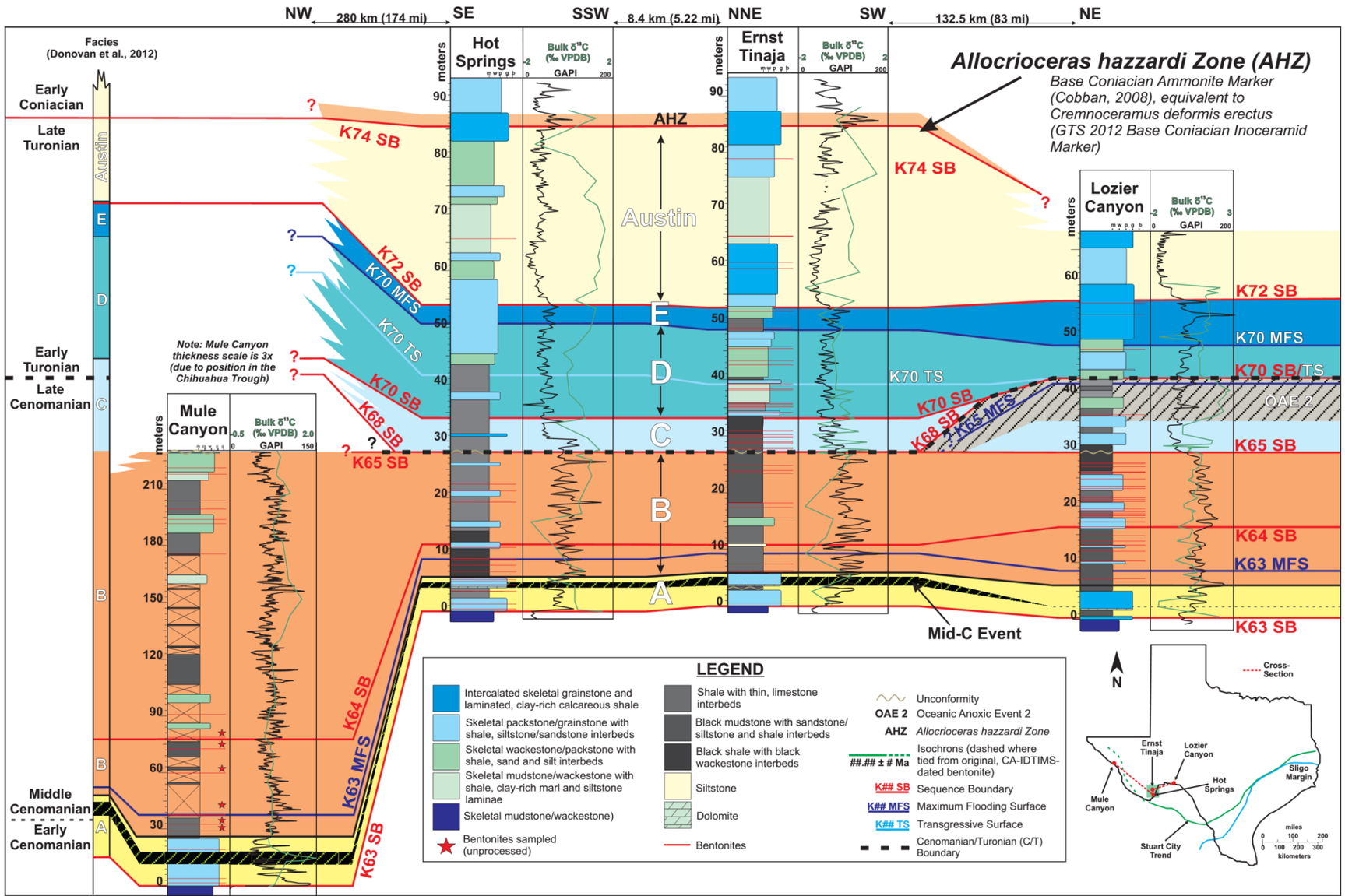

Figure 14. A facies model of the west Texas outcrops studied, including general age(s) of facies and position of the C/T boundary in all sections (facies after Donovan et al., 2012). Facies A, regarded as a highly diachronous facies, is nearly 30 m (100 ft) thick in the Ojinaga Formation (Mule Canyon) with thicknesses between 4.9-6.7 m (16-22 ft) on the carbonate platform. Facies B thicknesses are relatively consistent on the platform, and are significantly thicker in the Ojinaga Formation (Mule Canyon). The interval of Facies C preserved at Lozier Canyon also preserves the OAE2. Facies C is the most diachronous of the Eagle Ford-equivalent facies, and appears on either side of the LEF/UEF hiatus (associated with the K 65 SB at Big Bend and the K 70 SB at Lozier Canyon) In Big Bend, a section of Facies C is preserved which follows OAE2 deposition, and is not recorded at Lozier Canyon. Lower Langtry deposits (Facies D) are significantly thicker in Big Bend than Lozier Canyon, due to increased accommodation associated with high sea levels and differential subsidence. This facies interpretation includes an expanded Late Turonian volume of Austin Chalk probably not preserved at Lozier Canyon (and in fact, is only preserved in localities including the Maverick Basin near Del Rio, Texas). The *Allocrioceras hazzardi* Zone (AHZ) does not define the Eagle Ford/Austin Chalk-equivalent boundary, but defines the earliest Coniacian. If using timescales older than the GTS 2012 (Gradstein et al., 2012), the Eagle Ford/Austin Chalk-equivalent contact in west Texas is located stratigraphically within the interval highlighted above. Our pick for the Eagle Ford/Austin Chalk-equivalent boundary is at 52.7 m (173 ft) at Ernst Tinaja, 54 m (177 ft) and 56.3 (185 ft) at Lozier Canyon.

Sample Number	Age (Ma)*	Interpretation Method Used	Location	Bentonite Details
ET-BOQ-4	97.49 ± 0.12	Concordia Age	Ernst Tinaja	Thickness ~2.5 cm in outcrop. Zircons are common and large (**30-70 µm**), prismatic, subhedral to euhedral, clear with scattered inclusions.
ET-BOQ-7.50 m	95.99 ± 0.15	Concordia Age	Ernst Tinaja	Thickness ~0.8 cm in outcrop. Zircons are common and small (**10-30 µm**), acicular, euhedral, clear and contain few inclusions.
ET-BOQ-52.05 m	91.16 ± 0.16	Concordia Age	Ernst Tinaja	Thickness ~15.5 cm in outcrop. Zircons abundant, large (**90-270 µm**), prismatic to acicular, euhedral, clear and contain few inclusions.
HS-BOQ-2	**TBA**	Concordia Age	Hot Springs	Thickness ~0.4 cm in outcrop. Zircons are uncommon, very small (**10-15 µm**), prismatic, subhedral to euhedral, clear to pale yellow and contain few inclusions.
HS-BOQ-4	N/A (*insufficient zircon)*	N/A	Hot Springs	Thickness ~2.5 cm in outcrop. Zircons are uncommon, small (**10-30 µm**), prismatic, subhedral, clear and contain few inclusions.
HS-BOQ-4.55 m	**TBA**	Concordia Age	Hot Springs	Thickness ~1 cm in outcrop. Zircons are abundant, small (**5-30 µm**), prismatic, euhedral, clear and contain few inclusions.
HS-BOQ-51.00 m	Upper Pennsylvanian (undefined)	?	Hot Springs	Thickness varies 0-3 cm (nodular). Iron oxide gangue abundant. Zircons are small (**5-20 µm**), uncommon, prismatic, euhedral, clear to pale yellow and lacking inclusions; **detrital.**

Table 1. Sample summary of bentonites processed for CA-IDTIMS analysis. Exact sampling localities (including latitude and longitude coordinates and uncertainty radii for collection locales) are included in Table A-1.

Key nannos- Ernst-Tinaja section, Big Bend National Park

Member Equivalents	Age (pre-2008 Timescale)	Age (2012 Timescale)	CC Zones	UC Zones	formation equivalent (Staerker)	Sample Depth (ft.)	Sample Depth (m)	Total Abundance estimate (120 fov)	key markers used for correlation: Coralithion kennedyi	Helenia chiastia	Axapodorhabdus albianus	Rhagadiscus asper	Staurolithites aenigma	Eprolithus octopetalus	G. obliquum	Chiastozygus spissus	K. magnificus	Q. gartneri	Eprolithus eptapetalus (moratus)	Effellithus eximius (sensu strictu)	Lithastrinus septenarius	Miravetesina ficula	Aspidolithus parcus expansus	Micula decussata	nanno fossil picks	comments
Austin	Coniacian	Late Turonian	CC13b	UC9c	Austin	320	97.5	571	0	0	0	0	0	0	2	0	4	1	0	3	1	3	3	0	*section below FAD M.decussata*	
					Austin	311.5	94.9	826																		
					Austin	309.4	94.3	765																		
					Austin	298.7	91.0	2907	0	0	0	0	0	0	3	0	1	0	0	10	1	3	1			
					Austin	284.5	86.7	969																		
					Austin	280.5	85.5																			*not used - broken slide*
					Austin	270.7	82.5	3060	0	0	0	0	0	0	3	0	1	1	0	11	2	2	1	0		
					Austin	257	78.3	2652																		
					Austin	246.5	75.1	2315	0	0	0	0	0	0	1	0	1	1	0	7	1	1	1	0	**FAD A. parcusexpansa**	this event always falls in Austin within the region
				UC9a/b	Austin	236.5	72.1	2315																		
					Austin?	230.2	70.2	2703																		
Langtry					Langtry?	226	68.9	2111	0	0	0	0	0	0	0	0	1	10	0	12	1	0	0	0		
					Langtry?	215	65.5	2234	0	0	0	0	0	0	1	0	2	2	0	6	0	2	0	0		
					Langtry	205.5	62.6	1989	0	0	0	0	0	0	2	0	0	0	0	**3**	**2**	**2**	0	0	**FAD L. septenarius; FCO M. ficula**	this event formerly denoted the base of the Conicaian using the old timescales
	Turonian		CC13a?	UC8	Langtry	190.5	58.1	663																		
					Langtry	184.2	56.1	449	0	0	0	0	0	0	0	0	0	1	0	1	0	0	0	0		
					Langtry	173.7	52.9	479	0	0	0	0	0	0	0	0	0	1	0	0	0	**1**	0	0		
					Langtry	167.2	51.0	347																		
					Langtry	153.54	46.8	592	0	0	0	0	0	0	1	0	0	0	0	2	0	0	0	0		
					Langtry	147	44.8	459																		
		Middle Turonian	CC12?		Langtry	140	42.7	816	0	0	0	0	0	0	0	1	0	1	**1**	**2**	0	0	0	0	**LAD C.spissus; LAD E.eptapetalus**	
Scott Ranch					U.EagleFord?	123	37.5	867	0	0	0	0	0	0	1	1	0	3	1	0	0	1	0	0		
					U.EagleFord?	115.5	35.2	551	0	0	0	0	0	0	1	1	0	1	1	0	0	0	0	0		
		Early Turonian			U.EagleFord	115	35.1	653	0	0	0	0	0	**1**	**2**	1	1	3	1	0	0	0	0	0	**LAD E.octopetalus**	
					U.EagleFord	107	32.6	898	0	0	0	0	0	0	0	0	**1**	**1**	2	**2**	0	0	0	0	*FAD Q.gartneri (too high)* & K. magnificus	
					U.EagleFord	104	31.7	479	0	0	0	1	0	**1**	0	0	0	0	1	0	0	0	0	0	*E.octopetalus (too high)*	
					U.EagleFord	102.5	31.2	377	0	0	0	0	0	0	0	0	0	0	**1**	0	0	0	0	0	**E.eptapetalus in range- poor pres.**	interpreted to have approx. 1my gap in the record, which may contain C/T boundary
Antonio Creek	Middle-Late Cenomanian	Middle-Late Cenomanian	CC9c-10a?	UC3?	L.EagleFord	97.8	29.8	357	0	**1**	0	1	0	0	0	0	0	0	0	0	0	0	0	0	LAD H.chiastia	
					L.EagleFord	83	25.3	663	2	0	0	1	0	0	0	0	0	0	0	0	0	0	0	0	LAD C.kennedyi	
					L.EagleFord	49	14.9	867																		
					L.EagleFord	41.5	12.6	1836	1	2	0	2	0	0	0	0	0	0	0	0	**0**	0	0	0		
					L.EagleFord	32	9.8	439																		
					L.EagleFord	24.5	7.5	2142	0	1	0	2	1	0	0	0	0	0	0	0	0	0	0	0		
					L.EagleFord	19.5	5.9	459																		
					L.EagleFord	16	4.9	357	?	0	0	1	0	0	0	0	0	0	0	0	0	0	0	0	still above base C. kennedyi	

Table 2. Nannofossil assemblages and interpretation based on 38 preliminary scans (to evaluate preservation) and 22 detailed sample analyses. Blank rows (grey) are samples which were scanned, but not selected for detailed analysis. This interpretation was prepared for this manuscript by T.S. Staerker.

Member Equivalents	Age (pre-2008 Timescale)	Age (2012 Timescale)	Formation Equivalents (Peavey & Lundquist)	Sample Depth (ft)	Sample Depth (m)	Total weight <2 mm (g)	2 mm - 63 µm prep weight (g)	%2 mm - 63 µm post-wash	% washed away	Total Abundance	Benthic Abundance (%)	Foraminiferal Picks (J.J. Lundquist)										Comments
												Rotalipora cushmani	*Helvetotoboturncana helvetica*	*Praeglobotruncana stephani*	*Dicarinella hagni*	*Marginotruncana renzi*	*M. schneegansi*	*M. marginata*	*M. pseudolinneiana*	*M. marianosi*	*M. sigali*	*D. primitiva*	*D. convacata*	
Austin	Late Turonian	Austin		311.5	94.9	N/A	N/A	N/A	N/A		?											X	?	
Austin		Austin		309.4	94.3																			
Austin		Austin		298.7	91.0	11.48	3.07	26.74	73.26	700k+	~10							X	X			X		
Austin		Austin		284.5	86.7	19.43	5.78	29.75	70.25		0						X			X	X			Lack of *M. marginata*
Austin		Austin		280.5	85.5																			
Austin		Austin		270.7	82.5																			
Austin		Austin		257	78.3																			
Austin		Austin		246.5	75.1	17.46	3.32	19.01	80.99	700k+	16				X			X	X	X	X			
Austin		Austin		236.5	72.1																			
Austin?		Austin		230.2	70.2																			
Langtry?		Langtry		226	68.9																			
Langtry?		Langtry		215	65.5																			
Langtry		Langtry		205.5	62.6																			
Langtry		Langtry		190.5	58.1																			
Langtry		Langtry		184.2	56.1																			
Langtry		Langtry		173.7	52.9	11.16	4.12	36.92	63.08		0							X	X					
Langtry		Langtry		167.2	51.0																			
Langtry		Langtry		153.54	46.8	6.07	1.48	24.38	75.62		Trace				X		X							
Langtry		Langtry		147	44.8																			
Langtry		Langtry		140	42.7																			
Langtry	Middle Turonian	U. EagleFord?		123	37.5	17.3	4.73	27.34	72.66		1 - 2					X	X							
U. EagleFord?		U. EagleFord?		115.5	35.2																			
U. EagleFord?		U. EagleFord?		115	35.1																			
U. EagleFord	Early Turonian	U. EagleFord		107	32.6																			
U. EagleFord		U. EagleFord		104	31.7																			
U. EagleFord		U. EagleFord		102.5	31.2																			
U. EagleFord		U. EagleFord		97.8	29.8	8.86	2.41	27.20	72.80		0		X	X	X									
L. EagleFord	Middle - Late Cenomanian	L. EagleFord		83	25.3																			
L. EagleFord		L. EagleFord		49	14.9																			
L. EagleFord		L. EagleFord		41.5	12.6																			
L. EagleFord		L. EagleFord		32	9.8																			
L. EagleFord		L. EagleFord		24.5	7.5																			
L. EagleFord		L. EagleFord		19.5	5.9																			
L. EagleFord		L. EagleFord		16	4.9	0.61	0.15	24.59	75.41		6 - 7	X												
L. EagleFord		L. EagleFord		10	3.1	3.29	1.65	50.15	49.85		6 - 7	X												

Table 3. Foraminiferal assemblages and interpretation based on 10 detailed sample analyses. Blank rows (grey) are samples which were neither scanned nor analyzed. This interpretation was prepared by the primary author, based on information provided by J.J. Lundquist.

Stratigraphic Interval in Meters (feet)	COR-Derived MIN Sedimentation Rate (in cm/kyr (ft/myr))	COR-Derived MAX Sedimentation Rate (in cm/kyr (ft/myr))	COR-Derived AVG Sedimentation Rate (in cm/kyr (ft/myr))
52.05-84.8 (171.3-279.1)	1.80 (59.1)	3.64 (119.4)	2.72 (89.2)
47.3-52.05 (155.7-171.3)	0.46 (15.1)	1.16 (38.1)	0.81 (26.6)
27.2-47.3 (89.5-155.7)	1.24 (40.7)	3.24 (106.3)	2.24 (73.5)
22.3-27.2 (73.4-89.5)	0.34 (11.2)	1.17 (38.4)	0.75 (24.8)
16-22.3 (52.7-73.4)	0.66 (21.7)	3.94 (129.3)	2.3 (75.5)
16-22.3 (24.7-52.7)	N/A	N/A	1.65 (51.1)
1.5-7.5 (5.0-24.7)	0.36 (11.8)	0.93 (30.5)	0.65 (21.2)
0.3-1.5 (1.0-5.0)	N/A	N/A	0.35 (11.48)

Table 4. Correlation (COR) - derived sedimentation rates for the Ernst Member type section, Ernst Tinaja (BBNP). Min/Max sedimentation rates were not calculated for intervals 0.3-1.5 m and 16-22.3 m, due to significant temporal overlap of CA-IDTIMS error.

APPENDIX B

B.1 *Field Methods*

Seven research trips to Big Bend National Park, Brewster County, TX were planned and executed, including November 11–14, 2015 (reconnaissance), January 19–25, 2016 (sample collection), March 13–18, 2016 (sample collection and measured section at Ernst Tinaja, with bed-by-bed sampling interval of basal 4.6 m), April 15–19, 2016 (sample collection and measured section at Hot Springs, with 15 cm sampling interval), June 16–21, 2016 (sample collection and measured section at Ernst Tinaja, with 15 cm sampling interval), October 13-16, 2016 (additional sample collection, section measuring past AHZ) and November 18-20, 2016 (hand-held SGR, additional lithologic data). Proper collections permits granted by the National Park Service at BIBE were in effect from December 2015-January 2016 (BIBE-2015-SCI-0049), January 2016 through June 2016 (BIBE-2016-SCI-0004) and January 2016-December 2016 (BIBE-2016-SCI-0007) for the collection of multiple ash beds and select sampling from the Ernst Tinaja measured sections for micropaleontological, nannopaleontological, HHXRF and $\delta^{13}C_{carb}$ and $\delta^{18}O_{carb}$ analyses.

Prior to each arrival, advanced notice for 1) arrival time, 2) duration of stay in the park, 3) vehicle information (make/model, license plate number) and 4) names of research participants was submitted to the NPS dispatch office. The morning after each arrival to the park, I checked into the visitor center at Panther Junction to receive my park fee waiver (in the form of receipt) to attach to my windshield (and to verify my vehicle's status as a

research vehicle). This waiver was displayed in the lower left corner of the windshield during all work days, and was not removed until the morning after departure from the park. Operations on work days began between 7:00 (dawn) – 9:00 A.M., concluding anywhere between 5:00 P.M. and sundown (as late as 8:30 P.M.) Travel time from lodging (within 2.5 miles of Panther Junction) to either field area was 30-35 minutes (Hot Springs, via gravel road) to 50-55 minutes (Ernst Tinaja, via Old Ore Road (4WD-preferred, south entrance)). Once in the field area, frequent breaks were taken every 60-90 minutes (lasting 5-15 minutes) to hydrate, eat, rest and/or reapply sunscreen. Breaks were taken at a higher frequency between 10 am – 2 pm (peak insolation times, applicable to the trips in April and June) to avoid heat exhaustion and sun stroke.

B.1.1 *Ash Bed Collection*

Ash beds were sampled in the Ernst Member of the Boquillas Formation, stratigraphically between the Buda Limestone (bottom) and base of the *Allocrioceras hazzardi* Zone (top). Prior to sampling, the collection sites were brushed off by hand, hammer or cloth to reduce contamination. Collection site locality information is included in Table A-1. Once the collection sites were cleaned, ash beds were collected laterally across (and as close to the ground as possible) from the lowest in outcrop moving upward. This method was utilized to reduce sample contamination and minimize outcrop damage. Rock hammers, sledges and chisels were necessary to destroy overlying and/or underlying beds where accessibility of the ash bed was limited. Unfortunately, some of the ash beds collected were 1) indurated and lithified, 2) outcropping in vertical exposures, or 3) had high populations of brown recluse spiders living juxtapose to the ash beds, resulting in

increased difficulty in extraction and decreased sample yield (less than two gallons, and sometimes less than one in extreme cases). The best technique when collecting indurated beds was to find those freshly exposed and minimally covered by overlying beds. These samples, such as those within the Donovan Facies A-equivalent at Hot Springs and Ernst Tinaja, were the most difficult to recover and had the greatest contamination potential (from powdered residue of the now-destroyed overlying beds or close proximity of ash beds to one another). The easiest ash beds to recover were nodular in appearance or non-indurated, pinching in and out within micritic horizons or with thicknesses >20 mm. Nodular, intracarbonate ash beds pinch and swell laterally, sometimes shifting vertically in section by 5-10 cm or more. Nodular, intracarbonate ash beds which have vertical shifts in outcrop were ignored in this study, due to uncertainty in their temporal concordance relative to vertical position in section. Nodular, intracarbonate ash beds observed in Big Bend were often cemented with calcite, containing abundant loose material (iron oxides, calcite, etc.) in the nodule centers, suggesting their deposition is coincident with deposition of the carbonate bed in which they're preserved.

Two different labelling methods for bentonites sampled at Hot Springs and Ernst Tinaja were implemented. The first labelling scheme (used before the measured sections were generated) was locality name ("HS" for Hot Springs and "ET" for Ernst Tinaja), dash, formation name (Boquillas Formation (BOQ)), dash, ash bed number above the Buda Limestone/Ernst Member contact (x or xx, except where ash beds split or amalgamated (in which case, numbers like xa and xb were used). The second labelling

scheme was locality name (HS or ET), dash, formation name (BOQ), dash, position in section above Buda Limestone/Ernst Member contact (reported in m). Examples include:

Format 1	ET-BOQ-1, HS-BOQ-8a, HS-BOQ-10
Format 2	ET-BOQ-4.55m, HS-BOQ-51.00m

A Garmin eTrex 10 Hiking GPS Navigator (v. 2.2) was used unsuccessfully to provide exact latitude and longitude coordinates for sample collection sites (signal absent from satellites). Measured section positions (for segment ends) were delineated by satellite imagery using the GeoLocate Web Application (http://www.museum.tulane.edu/geolocate/web/WebGeoref.aspx), developed and maintained by Tulane University. Below is a list of the samples collected (with corresponding locality information) which yielded ash bed ages:

Sample Number	Latitude	Longitude	Uncertainty Radius (m)
HS-BOQ-4	29.18229	-102.9933598	8
HS-BOQ-4.55m	29.18266	-102.993666	3
HS-BOQ-51.00m	29.18214	-102.995623	10
ET-BOQ-4	29.25616	-103.011695	3
ET-BOQ-7.50m	29.25608	-103.011965	6
ET-BOQ-52.05m	29.25553	-103.013496	2

Table A-1. Latitude, longitude and uncertainty radius data for ash beds collected which yielded ages after laboratory processing of sample (via the CA-TIMS (ID-TIMS) methodology).

B.1.2 *Photographs*

Photography in the park was taken by Samsung Galaxy S4 and Samsung Galaxy S5 androids at the Hot Springs and Ernst Tinaja field sites. Requests for photographs may be directed to eric_peavey@tamu.edu. If I don't respond within 1-2 business days, please send your request to eric.j.peavey@gmail.com, as my institutional e-mail will likely be terminated shortly after my graduated status is granted by Texas A&M University. Additional high-resolution photographs (from a Canon EOS 60D, with 35mm lens and Auto-White Balance) are available.

B.1.3 *Measured Sections*

The major assumption contributing to the thicknesses of my measured sections is the position of the contact between the Ernst Member and the overlying San Vicente Member, which I interpret to be at the base of the *Allocrioceras hazzardi* Zone. My sections were measured from the basal Ernst (at the Buda Limestone/Ernst Member contact) to the base of the *Allocrioceras* beds. Three measured sections were generated, with the first in March (Ernst Tinaja, bed-by-bed), second in April (Hot Springs, sampling interval 15 cm) and third in June (Ernst Tinaja, sampling interval 15 cm). Latitude and longitude coordinates for each segment end as well as lithology measurements and notes/comments (recorded verbatim from field notebooks), are available in the excel spreadsheet at the end of the appendix (under the Supporting Data header).

B.1.3.1 *Measured Section 1 (Ernst Tinaja, March 15, 2016)*

Two sections were measured at Ernst Tinaja up vertical exposures in the Ernst Tinaja arroyo. The first section was a high resolution, bed-by-bed measurement of the first

4.6 m of the Ernst Member, generated to record the high frequency lithologic shifts in sediment deposition throughout the study interval. A 1.5 meter, metric Tailor Ruler was used to measure lamina and bed thicknesses. In all, 189 beds (including 15 ash beds and excluding hundreds of laminae finer than the 0.1 mm measuring resolution) were documented, with laminae/bed thicknesses ranging from 0.1 mm to more than 8 cm (including the oyster zone near the top of the Facies A-equivalent). This section could be utilized for astrochronologic analysis, and would serve as a means of testing the veracity of the chronostratigraphic framework presented in this study. The second section, measured through the entire thickness of the Ernst Member of the Boquillas Formation at Ernst Tinaja, BBNP is discussed in the Methods section.

B.1.3.1.1 *Locality Information*

Ernst Tinaja is located within Cuesta Carlota (small mountain range), 4.65 miles along Old Ore Road (measured from the south entrance) and about .45 miles down the canyon from the northern edge of the Ernst Tinaja parking area (visible in satellite view, about 0.36 miles NE of the fork in Old Ore Road, 4.65 miles from the southern entrance).

B.1.3.2 *Measured Section 2 (Hot Springs, April 16-17, 2016)*

The first measured section at Hot Springs was measured in three segments (with two lateral shifts), traversing 240-285 azimuth (SW to WNW), corresponding to and trending along local dip. This section had a 15-centimeter sampling interval. A metal Jacob's Staff and Brunton Compass were used to measure 1.65 meter increments in the section. Red caution flags were placed into the ground in 1.65 meter increments throughout the section. Photographs of outcrop and sampling were taken in lieu of

collecting hand samples. A 15 foot, imperial unit measuring tape was used to measure lamina and bed thicknesses. In some cases, sampling increments were difficult to determine, especially where outcrops were not visible and left a consistent topographic grade from flag to flag. If this occurred, the measuring tape was extended between two flags (after verifying consistency of the topographic grade between them with the Jacob's Staff), with the measuring tape being held horizontally. The horizontal distance between the flags (equivalent aerial distance) was divided into eleven sampling points to obtain equally-spaced sampling positions (laterally and vertically). Sampling positions without obvious outcrops are labelled as "(slope)" in the Supporting Data section and were treated as covered section.

B.1.3.2.1 *Locality Information*

The Hot Springs locality is located within .5 miles of the Rio Grande River in Big Bend National Park and is more difficult to get to than Ernst Tinaja. The main road between Panther Junction and Boquillas Village (Park Rte 12) has a road about 1.07 miles west (along road) of the intersection of Park Rte. 12 and Old Ore Road. Signs leading to "Hot Springs" are posted for visibility. At the end of this gravel road, there's a parking area (with restrooms). The field area can be accessed by travelling about 0.55 miles east from the eastern edge of the Hot Springs parking area along the Hot Springs Trail. A small knoll with bushes/trees with exposed outcrops in a small stream valley is about 80' N70W of the trail, just before it makes a 90° bend trending eastward. This outcrop is where the first segment of the section was measured.

B.2 *Laboratory Methods*

B.2.1 *Ash Bed Processing*

The processing of ash beds into zircons (and thus, geologic ages we can use for chronocorrelation of strata in local and regional frameworks) incorporates several steps and requires sedulous attention to sources of contamination and adherence to strict laboratory procedures. Physical copies of a comprehensive, step-by-step reference guide for the ash bed processing techniques utilized for the completion of this research is available in multiple labs within TAMU's Geology and Geophysics Department. For inquiries related to the exact procedure or for a physical copy of the reference guide, please contact Dr. Brent V. Miller (bvmiller@geo.tamu.edu). Chemical Abrasion methods are provided in Appendix B.2.3.

B.2.2 *Cleaning*

The operating assumption while working in the rock lab, mineral separation lab and clean lab is that all surfaces, tools, equipment and clothing are contaminated immediately upon arrival into the working area. Any motorized equipment (jaw crusher, pulverizer, and Wilfley (water) table) must be thoroughly washed with soapy water, rinsed and dried, then doused in ethanol and treated with compressed air to reduce rusting. This cleaning process, ideally, should take 90-120 minutes for the jaw crusher/pulverizer, and 45 minutes for the Wilfley table. Time spent cleaning is dependent on the number of parts in the motorized equipment (e.g., plates, screws and washers for the jaw crusher, discs, screws and washers for the pulverizer or sieves and steamtable buckets for the Wilfey

table). Cleaning times may increase (and sometimes double) due to complications with sticky samples or contamination concerns.

B.2.3 *Chemical Abrasion Methods*

Large rock fragments were reduced to gravel size using the Badger Jaw Crusher, then crushed using the Bico disc pulverizer to fragments <2 mm in diameter. Repeated treatment of ash beds with soapy water and 12 M (or ~50%) HCl disaggregated clays and dissolved extraneous carbonate in each sample. Once crushed, each sample was sieved to <1 mm diameter and processed through the Wilfley (water) table to separate heavy and light mineral fractions. In some cases, the volume of heavy fraction is substantial, and must be reduced further by processing through the Frantz machine (which utilizes a strong magnetic field to separate magnetic/paramagnetic minerals from zircons, apatites and other non-magnetic, dense minerals). The resulting magnetic/non-magnetic fractions were treated with methylene iodide (MEI) to produce clear mineral density separation within the remaining volume of material. This process produced both a 'heavy' and 'light' mineral fraction for each sample. Light mineral fractions were preserved for potential need for sample reprocessing.

Zircons were then picked from the heavy fraction (using a petrographic microscope) and annealed at a temperature of ~900°C for 90 hours in a Barnstead Thermolyne 1400 Furnace. Once annealed, zircons were selected based on 1) optical clarity, 2) their being euhedral, and 3) absence of fractures and inclusions (under plane polarized light) and later photographed. Cathodoluminescence imaging was not utilized for potential verification of xenocrystic cores and/or complex zoning in selected zircons.

As many as eighteen 'ideal' zircons per sample were placed into 200 μL Teflon microcap capsules with HF and placed into a Parr-type high-pressure dissolution vessel (e.g., bomb) and heated for 72 hours or more at ~210 °C in the FisherScientific™ Isotemp™ Gravity Oven (AISI 430/1.4016). The 205Pb-233U-235U spikes used for U-Pb analysis were calibrated with reference to two separate external spike calibration solutions and the EarthTime nominal 100 Ma, 500 Ma and 2 Ga laboratory standards.

Once dissolved, sample solutions were loaded onto Teflon microcolumns with ElChrom® anion resin, which initially washed Zr, Hf and rare earth elements (REEs) before bifurcation of U and Pb by HCl. The segregated U and Pb were loaded on degassed Rhenium (Re) filaments using 1 μL of silicic acid loading solution (gel). Each original 18-grain zircon yield produced up to 18 sample solutions, which were loaded onto each of the 18 Re filaments along with two blanks onto the sample turret. All measurements were generated using a ThemoFisher™ Triton Thermal-Ionization Mass Spectrometer (TIMS). Best-age interpretations are reported in the form X ± Y (Z) Ma, where X is the mean of the best-age interpretation, Y is the 2σ error including systematic error in decay constants, and Z is the 2σ error excluding uncertainty in the decay constant. The Y-form error should be used when comparing ages determined using different methods (e.g., $^{40}Ar/^{39}Ar$), and Z-form error used when making comparisons between the determined age and relative astrochronology-determined age (Schoene et al., 2006). Final ages may be determined by using Concordia diagrams or regression analyses of some number of youngest grains in a sample. Data reduction and construction of Concordia diagrams were performed by Brent V. Miller using Excel templates and IsoPlot, respectively.

B.2.4 *Hand-held Scintillometer Methods*

For the third measured section, two hand-held Terraplus RS-230 scintillometers were used, alternating measurements at a 0.3 m (1 ft) spacing from 1.6 m (-5 ft, within the Buda Limestone) to 93.2 m (306 ft; ~30 feet above the base of the San Vicente Member). The hand-held scintillometers were frequently calibrated to the surrounding air at Ernst Tinaja due to the instruments' sensitivity of calibration to fluctuating weather conditions.

APPENDIX C

C.1 *Supplemental Data for CA-IDTIMS Age-Dating*

For raw data, Concordia plots and CA-IDTIMS-dated bentonites for samples HS-BOQ-2 and HS-BOQ-4.55 m, please contact Brent V. Miller at bvmiller@geo.tamu.edu.

C.2 *Spreadsheets (Litho-, Bio- and Chemostratigraphy)*

An excel workbook containing field notes from all measured sections generated at Big Bend is attached as a separate .xlsx (Excel 2013) file with this manuscript (Appendix C). All detailed data collected for lithostratigraphy, sedimentary structures, HHSGR, stable isotopes, nannofossils and foraminifera are provided as separate tabs. XRF plots of all trace element concentrations are also provided. A second spreadsheet, with raw and reduced data, and Concordia diagrams for bentonite samples is included.

If you wish to obtain an electronic copy of the data, please direct your inquiries to eric_peavey@tamu.edu. If I don't respond within 1-2 business days, please send your request to eric.j.peavey@gmail.com, as my institutional e-mail will likely be terminated shortly after granted a 'graduated' status by Texas A&M University.

C.3 *Future Work*

The sequence stratigraphic (stratal surface) interpretations presented in this paper include one of two working hypotheses, with major points of contention and questions including:

1. The origin and nomenclatural assignment of Early Cenomanian strata overlying the Buda Limestone in the first 9 (30), 2.8 (9), 2.6 (8) and 0.9 (3) m (ft) at Mule Canyon, Hot Springs, Ernst Tinaja and Lozier Canyon, respectively.
    a. Do these Early Cenomanian strata belong to the Lower Eagle Ford, Pepper Shale, Maness Shale, Woodbine Group or False Buda formational equivalents?
2. The origin and exact duration of the hiatus straddling the LEF/UEF at Big Bend, and within the UEF at Lozier Canyon.
    a. Possible origins of a large hiatus in a carbonate-dominated formation include:
        i. Palaeoceanographic conditions favorable for the spontaneous dissolution of calcium carbonate at the sediment-water interface (requiring undersaturation of $CaCO_3$ in the water column, low pH and high activation energy for the reaction).
        ii. A forebulge migration, trending NW-SE, which moves northeastward following Sevier deformation (and is coincident with the collision of the Farallon and Kula plates with the North American Plate) and is coincident with the development of a hiatus spanning the Late Cenomanian – Middle Turonian in the central western interior (White et al., 2002).
        iii. The development of a regional-scale ravinement surface, facilitated by a rapid, episodic connection and disconnection of the Boreal and Tethys arms of the Western Interior Seaway and subsequent scouring by cool, Boreal waters across the platform, leading to transport and deposition of material into the Chihuahua Trough and Sabinas Basin.

3. The significance of the ~25’ of C-facies, latest Early Turonian deposition in Big Bend, coincident with the recovery period immediately following OAE2.
    a. Should the interpreted C-facies strata be lumped with the Middle Turonian, D-facies lowstand wedge deposits above? If so, what’s the mechanism contributing to increased accommodation in the early Middle Turonian at Big Bend?
4. The temporal assignment of an interval of Austin Chalk-equivalent strata, spanning ~52.7–84.6 m (173–277.5 ft) at BBNP.

According to the GTS 2004 (Ogg et al., 2004), this interval lies in the Coniacian. Conversely, the GTS 2012 (Gradstein et al., 2012) places this volume in the Late Turonian, following middle Late Turonian deposition of Eagle Ford-equivalent strata (bounded below by a 91.16 ± 0.16 Ma bentonite age).